NACA TN 3205 9457

TECH LIBRARY KAFB, NM
0066067

NATIONAL ADVISORY COMMITTEE FOR AERONAUTICS

TECHNICAL NOTE 3205

THEORETICAL INVESTIGATION AT SUBSONIC SPEEDS OF THE FLOW AHEAD OF A SLENDER INCLINED PARABOLIC-ARC BODY OF REVOLUTION AND CORRELATION WITH EXPERIMENTAL DATA OBTAINED AT LOW SPEEDS

By William Letko and Edward C. B. Danforth, III

Langley Aeronautical Laboratory
Langley Field, Va.

Washington
July 1954

AFMDC
TECHNICAL
AFL 25

ERRATA

NACA TN 3205

THEORETICAL INVESTIGATION AT SUBSONIC SPEEDS
OF THE FLOW AHEAD OF A SLENDER INCLINED PARABOLIC-ARC
BODY OF REVOLUTION AND CORRELATION WITH EXPERIMENTAL
DATA OBTAINED AT LOW SPEEDS

By William Letko and Edward C. B. Danforth, III

July 1954

Page 10: Equation (20) should be replaced by the following equation, in which two errors in sign are corrected:

$$w_2 \approx -\frac{VB^2\alpha \sin\theta}{F^2}\left\{\frac{\sqrt{(x-1)^2+B^2r^2}}{B^2r^2}\left(\frac{x^3+x^2-x-1}{2}-\frac{13}{4}xB^2r^2-\frac{3}{4}B^2r^2\right)-\right.$$

$$\frac{\sqrt{(x+1)^2+B^2r^2}}{B^2r^2}\left(\frac{x^3-x^2-x+1}{2}-\frac{13}{4}xB^2r^2+\frac{3}{4}B^2r^2\right)+$$

$$\left.\left(3x^2-\frac{3}{4}B^2r^2-1\right)\left[\sinh^{-1}\left(\frac{x-1}{Br}\right)-\sinh^{-1}\left(\frac{x+1}{Br}\right)\right]\right\} \qquad (20)$$

TECH LIBRARY KAFB, NM
0066067

NATIONAL ADVISORY COMMITTEE FOR AERONAUTICS

TECHNICAL NOTE 3205

THEORETICAL INVESTIGATION AT SUBSONIC SPEEDS OF THE FLOW AHEAD OF A SLENDER INCLINED PARABOLIC-ARC BODY OF REVOLUTION AND CORRELATION WITH EXPERIMENTAL DATA OBTAINED AT LOW SPEEDS

By William Letko and Edward C. B. Danforth, III

SUMMARY

Subsonic linearized theory is used to derive approximate expressions for the incremental pressure coefficient and flow inclination ahead of slender parabolic-arc bodies of revolution alined with the stream and at small angles of attack or sideslip.

Numerical results are presented in the form of charts which permit the rapid estimation of the deviations from free-stream values of static pressure, angle of attack, and angle of sideslip so that suitable positions for orifices and vanes for measuring these quantities can readily be selected. Comparisons between calculated values and those measured at a Mach number of 0.21 for a body of fineness ratio 6 show that for distances greater than 1/2 body diameter in front of the body nose and for angles of attack less than 20° the approximate theory used herein is adequate for predicting the best location for static-pressure and angle-measuring pickups.

The effect of wing lift and mounting-boom interference on the angle-of-attack indication as determined from a simple theory is also presented. The calculations show that the angle-of-attack deviation introduced by the wing may be large for some configurations and should be considered in determining a suitable location for an angle-measuring pickup.

INTRODUCTION

In the instrumentation of airplanes, particularly for research purposes, it is often desirable to measure static pressure and angles of attack and sideslip by locating static orifices and freely floating vanes ahead of the nose of the body. The values of the static pressure and the angles of attack and sideslip which are measured are rarely the free-stream

values since the flow ahead of the body deviates from the free-stream static pressure and direction. The accepted practice is to locate the orifices and the vanes at a sufficient distance from the body nose so that the deviations encountered will be small. The installation is then calibrated in flight to determine the magnitude of the residual errors and their variation with Mach number.

It is the purpose of this paper to determine the flow deviations ahead of a body in order that the increments due to the body in static pressure and in angles of attack and sideslip can be estimated for orifices and vanes located anywhere in the flow field ahead of the body. Subsonic linearized theory has been utilized to calculate the flow ahead of a simple sharp-nosed body of revolution of arbitrary fineness ratio. The meridian lines of the body have been chosen as parabolic arcs for ease of calculation.

In order to show in what ranges of location and angle of attack the theory is valid, experimental measurements of static pressure and flow angularity were made at a Mach number of 0.21 ahead of a parabolic-arc body of fineness ratio 6 and are presented herein.

SYMBOLS

A	wing aspect ratio
a	radius of body nose boom
$B = \sqrt{1 - M^2}$	
C_{L_α}	lift-curve slope
F	fineness ratio of body, $\frac{l}{\text{Maximum diameter}}$
l	length of body
M	free-stream Mach number
p	static pressure
p_o	free-stream static pressure
q	free-stream dynamic pressure

$\frac{\Delta p}{q}$	pressure coefficient, $\frac{p - p_o}{q}$
$\left(\frac{\Delta p}{q}\right)_1$	incremental pressure coefficient due to body thickness
$\left(\frac{\Delta p}{q}\right)_2$	incremental pressure coefficient due to body angle of attack
r_B	radial coordinate of body surface
s	wing semispan
S	cross-sectional area of body
u,v,w	axial, radial, and tangential velocity components
u_1	axial disturbance velocity due to body thickness
u_2	axial disturbance velocity due to body angle of attack
V	free-stream velocity
v_H	horizontal disturbance velocity due to body angle of attack (see fig. 1(a))
v_V	vertical disturbance velocity due to body angle of attack (see fig. 1(a))
v_1	radial disturbance velocity due to body thickness
v_2	radial disturbance velocity due to body angle of attack
w_2	tangential disturbance velocity due to body angle of attack
w_W	wing induced upwash velocity
x,r,θ	cylindrical coordinate system
x'	axial coordinate in Cartesian coordinate system
α	angle of attack
α_i	angle of attack indicated by vane
$\Delta\alpha$	increment in angle of attack

β	angle of sideslip
$\Delta\beta$	increment in angle of sideslip
Γ	circulation
ξ	variable of integration along axis of body
ρ	mass density of air
ϕ	disturbance velocity potential
ϕ_1	disturbance velocity potential due to body thickness
ϕ_2	disturbance velocity potential due to body angle of attack

APPLICATION OF THEORY

Basic Theory

The linearized equation governing subsonic potential flow in general cylindrical coordinates may be written in terms of the disturbance velocity potential as

$$B^2 \frac{\partial^2\phi}{\partial x^2} + \frac{\partial^2\phi}{\partial r^2} + \frac{1}{r}\frac{\partial\phi}{\partial r} + \frac{1}{r^2}\frac{\partial^2\phi}{\partial\theta^2} = 0 \tag{1}$$

It is well-known that the general solution of equation (1) representing the flow about slender bodies of revolution at a small angle of attack with respect to the stream may be written as

$$\phi = \phi_1 + \phi_2 \tag{2}$$

where ϕ_1 and ϕ_2 are the disturbance velocity potentials that represent the thickness and angle-of-attack effects, respectively. The solution ϕ_1 representing the thickness effect is given in reference 1 as

$$\phi_1 = -\frac{V}{4\pi}\int \frac{S'(\xi)}{\sqrt{(x-\xi)^2 + B^2r^2}}\,d\xi \tag{3}$$

In equation (3) the function $S'(\xi)$ defines the source distribution in terms of the axial rate of change of cross-sectional area. The cross-sectional area is given by $S = \pi r_B^2$ and the integration is to be made over the length of the body.

The disturbance velocity potential ϕ_2 represents the part of the flow disturbance resulting from the angle of attack and is given in reference 2 by

$$\phi_2 = -\frac{Br\cos\theta}{4\pi}\int\frac{g(\xi)}{\left[(x-\xi)^2 + B^2r^2\right]^{3/2}}\,d\xi \tag{4}$$

where $\cos\omega$ in reference 2 is replaced by $-\cos\theta$. (This change in notation has been made to maintain a consistant sign convention.) For slender bodies, the function $g(\xi)$, representing the required doublet strength distribution, is shown in reference 2 to be

$$g(\xi) = 2V\alpha B\,S(\xi)\left[1 - B^2\frac{S''(\xi)}{2\pi}\log\frac{r_B(\xi)}{l}\right] \tag{5}$$

where $r_B(\xi)$, $S(\xi)$, and $S''(\xi)$ are functional relationships analagous to $S'(\xi)$ discussed previously.

Specific Application to Parabolic-Arc Bodies of Revolution

In this paper the theory has been used to calculate the flow ahead of the simple parabolic-arc body of revolution shown in figure 2. The meridian lines of the body have been chosen as parabolic arcs for ease of calculation. The cross-sectional area of the body is given by

$$S(x) = \frac{\pi}{F^2}\left(1 - x^2\right)^2$$

where F is the fineness ratio of the body and the nose and tail of the body have been chosen for convenience at $x = -1$ and 1, respectively, that is $l = 2$. (For bodies of arbitrary length, x is to be measured in half body lengths.) For convenience of presentation, the thickness and angle-of-attack effects on the flow ahead of the body are discussed separately.

Effects of thickness.- For the parabolic-arc body of revolution, equation (3) becomes

$$\phi_1 = -\frac{V}{F^2}\int_{-1}^{1} \frac{\xi^3 - \xi}{\sqrt{(x - \xi)^2 + B^2r^2}}\, d\xi \tag{6}$$

The axial and radial components of the disturbance velocities are given by

$$u_1 = \frac{\partial \phi_1}{\partial x} = \frac{V}{F^2}\int_{-1}^{1} \frac{(x - \xi)(\xi^3 - \xi)}{\left[(x - \xi)^2 + B^2r^2\right]^{3/2}}\, d\xi \tag{7}$$

and

$$v_1 = \frac{\partial \phi_1}{\partial r} = \frac{VB^2r}{F^2}\int_{-1}^{1} \frac{\xi^3 - \xi}{\left[(x - \xi)^2 + B^2r^2\right]^{3/2}}\, d\xi \tag{8}$$

respectively.

Pressure coefficient: The pressure coefficient at a general point in the flow field ahead of the body may be adequately approximated by the expression $\left(\frac{\Delta p}{q}\right)_1 = -\frac{2u_1}{V}$. (The additional terms usually appearing in the correct linearized approximation for the pressure may be neglected in the present analysis without incurring any significant error.) Upon integration of equation (7), the pressure coefficient may be written as follows:

$$\left(\frac{\Delta p}{q}\right)_1 = \frac{3}{F^2}\left\{(1 + 3x)\sqrt{(x - 1)^2 + B^2r^2} + (1 - 3x)\sqrt{(x + 1)^2 + B^2r^2} + \left(2x^2 - B^2r^2 - \frac{2}{3}\right)\left[\sinh^{-1}\left(\frac{x + 1}{Br}\right) - \sinh^{-1}\left(\frac{x - 1}{Br}\right)\right]\right\} \tag{9}$$

Along the extended axis of the body, ahead of the body nose $(r=0, x<-1)$, equation (9) reduces to

$$\left(\frac{\Delta p}{q}\right)_1 = \frac{2}{F^2}\left[6x - \left(3x^2 - 1\right) \log \frac{x + 1}{x - 1}\right] \tag{10}$$

In equations (9) and (10) it is to be noted that x and r are nondimensional distances expressed as fractions of the half body length. Furthermore, x is measured from the midlength position of the body and is negative in the upstream direction. The static-pressure coefficient due to body thickness calculated from equation (9) is presented in figure 3.

Flow inclination: The flow inclination, with respect to the axis of the body, caused by body thickness can be obtained by integrating equation (8) as

$$\frac{v_1}{V} = \frac{B}{F^2}\left\{\left(x^2 - x - 2B^2r^2\right) \frac{\sqrt{(x + 1)^2 + B^2r^2}}{Br} - \left(x^2 + x - 2B^2r^2\right) \frac{\sqrt{(x - 1)^2 + B^2r^2}}{Br} + 3xBr\left[\sinh^{-1}\left(\frac{x + 1}{Br}\right) - \sinh^{-1}\left(\frac{x - 1}{Br}\right)\right]\right\} \tag{11}$$

Values of $\frac{v_1}{V}$ can be obtained from figure 4 which was prepared by use of equation (11).

Effects of angle of attack.- The axial, radial, and tangential velocity components caused by angle of attack are given by

$$\left.\begin{aligned} u_2 &= \frac{\partial \phi_2}{\partial x} \\ v_2 &= \frac{\partial \phi_2}{\partial r} \\ w_2 &= \frac{1}{r}\frac{\partial \phi_2}{\partial \theta} \end{aligned}\right\} \tag{12}$$

Pressure coefficient: That part of the pressure coefficient caused by the inclination of the body may be adequately approximated in the present analysis by $\left(\frac{\Delta p}{q}\right)_2 = -\frac{2u_2}{V}$ (see previous discussion for $\left(\frac{\Delta p}{q}\right)_1$). Using this relationship and equations (4), (5), and (12) and performing the indicated operations gives the following equation for the pressure coefficient due to body angle of attack:

$$\left(\frac{\Delta p}{q}\right)_2 = -\frac{2}{V}\frac{\partial \phi_2}{\partial x}$$

$$= -\frac{3B^2 r\alpha \cos\theta}{F^2}\int_{-1}^{1}\frac{(1-\xi^2)^2(x-\xi)}{\left[(x-\xi)^2 + B^2r^2\right]^{5/2}}\,d\xi -$$

$$\frac{6B^4 r\alpha \cos\theta}{F^4}\int_{-1}^{1}\frac{(1-\xi^2)^2(1-3\xi^2)(x-\xi)\log\frac{1-\xi^2}{2F}}{\left[(x-\xi)^2 + B^2r^2\right]^{5/2}}\,d\xi \qquad (13)$$

Because the integral which forms the second part of equation (13) is rather involved, it was solved graphically to determine the importance of its contribution to the complete pressure coefficient. The solution was obtained for a body of fineness ratio 6 and $B = 0.98$ (that is, $M = 0.21$) and indicates (see fig. 5) that the use of only the first term of equation (13), approximate solution, would give values of $\left(\frac{\Delta p}{q}\right)_2$ which, for reasonable distances from the body, would not differ appreciably from those obtained by use of the complete equation. Although the graphical solution was obtained only for a body of fineness ratio 6 and for a Mach number of 0.21, examination of equation (13) indicates that neglecting the second term of equation (13) would affect the estimates even less for bodies with higher fineness ratios or for flow at larger Mach numbers.

Integration of the first term of equation (13) yielded the following formula for the pressure coefficient:

$$\left(\frac{\Delta p}{q}\right)_2 \approx \frac{4B\alpha\cos\theta}{F^2}\left\{\left(x^2 - x - 2B^2r^2\right)\frac{\sqrt{(x+1)^2 + B^2r^2}}{Br} - \left(x^2 + x - 2B^2r^2\right)\frac{\sqrt{(x-1)^2 + B^2r^2}}{Br} + 3xBr\left[\sinh^{-1}\left(\frac{x+1}{Br}\right) - \sinh^{-1}\left(\frac{x-1}{Br}\right)\right]\right\} \qquad (14)$$

Values of $\left(\frac{\Delta p}{q}\right)_2$ ahead of the body can be estimated from figure 4 for values of Br from 0.05 to 0.4.

Flow inclination: The disturbance velocity due to body angle of attack that affects angle-of-attack measurements v_V is given by (see fig. 1(a))

$$v_V = w_2 \sin\theta - v_2 \cos\theta \tag{15}$$

and the disturbance velocity due to body angle of attack that affects the angle-of-sideslip measurements v_H is given by

$$v_H = w_2 \cos\theta + v_2 \sin\theta \tag{16}$$

For parabolic-arc bodies of revolution, the following solutions for v_2 and w_2 are obtained by using equations (4), (5), and (12) and by performing the indicated operations:

$$v_2 = -\frac{\alpha V B^2 \cos\theta}{2F^2}\int_{-1}^{1}\left(1-\xi^2\right)^2 \frac{(x-\xi)^2 - 2B^2r^2}{\left[(x-\xi)^2 + B^2r^2\right]^{5/2}}\,d\xi + \frac{\alpha V B^4 \cos\theta}{F^4}\int_{-1}^{1}\left(1-\xi^2\right)^2\left(3\xi^2-1\right)\frac{(x-\xi)^2 - 2B^2r^2}{\left[(x-\xi)^2 + B^2r^2\right]^{5/2}}\log\frac{1-\xi^2}{2F}\,d\xi \tag{17}$$

and

$$w_2 = \frac{\alpha V B^2 \sin\theta}{2F^2}\int_{-1}^{1}\frac{\left(1-\xi^2\right)^2}{\left[(x-\xi)^2 + B^2r^2\right]^{3/2}}\,d\xi - \frac{\alpha V B^4 \sin\theta}{F^4}\int_{-1}^{1}\frac{\left(1-\xi^2\right)^2\left(3\xi^2-1\right)}{\left[(x-\xi)^2 + B^2r^2\right]^{3/2}}\log\frac{1-\xi^2}{2F}\,d\xi \tag{18}$$

It was found that neglecting the second terms of equations (17) and (18) would not result in an appreciable difference in the estimated values of v_2 and w_2 for practical distances ahead of the body (see figs. 6 and 7). The second terms of these equations were therefore neglected.

Integrating the first terms of equations (17) and (18) results in

$$v_2 \approx -\frac{V\alpha \cos\theta}{2F^2r^2}\left\{\left[x^3 + x^2 - \left(1 + \frac{23}{2}B^2r^2\right)x - \left(1 - \frac{9}{2}B^2r^2\right)\right]\sqrt{(x-1)^2 + B^2r^2} - \left[x^3 - x^2 - \left(1 - \frac{23}{2}B^2r^2\right)x + \left(1 - \frac{9}{2}B^2r^2\right)\right]\sqrt{(x+1)^2 + B^2r^2} - B^2r^2\left(6x^2 - 2 - \frac{9}{2}B^2r^2\right)\left[\sinh^{-1}\left(\frac{x-1}{Br}\right) - \sinh^{-1}\left(\frac{x+1}{Br}\right)\right]\right\} \quad (19)$$

and

$$w_2 \approx \frac{VB^2\alpha \sin\theta}{F^2}\left\{\frac{\sqrt{(x-1)^2 + B^2r^2}}{B^2r^2}\left(\frac{x^3 + x^2 - x - 1}{2} - \frac{13}{4}xB^2r^2 - \frac{3}{4}B^2r^2\right) - \frac{\sqrt{(x+1)^2 + B^2r^2}}{B^2r^2}\left(\frac{x^3 - x^2 - x + 1}{2} - \frac{13}{4}xB^2r^2 + \frac{3}{4}B^2r^2\right) - \left(3x^2 - \frac{3}{4}B^2r^2 - 1\right)\left[\sinh^{-1}\left(\frac{x-1}{Br}\right) - \sinh^{-1}\left(\frac{x+1}{Br}\right)\right]\right\} \quad (20)$$

Values of v_2 and w_2 can be determined from figures 8 and 9 which were prepared by using equations (19) and (20). On the extended axis of the body, ahead of the body nose, equations (19) and (20) reduce to

$$v_2 \approx \frac{V\alpha B^2 \cos\theta}{F^2}\left[\left(3x^2 - 1\right)\left(\log\frac{x+1}{x-1}\right) - 6x\right] \quad (21)$$

and

$$w_2 \approx -\frac{V\alpha B^2 \sin\theta}{F^2}\left[\left(3x^2 - 1\right)\left(\log\frac{x+1}{x-1}\right) - 6x\right] \quad (22)$$

Upon substitution of equations (21) and (22) into equations (15) and (16), the vertical and horizontal disturbance velocities on the body axis due to the angle of attack of the body may be expressed as

$$\left.\begin{aligned} v_V &= -\frac{V\alpha B^2}{F^2}\left[\left(3x^2 - 1\right)\left(\log\frac{x+1}{x-1}\right) - 6x\right] \\ v_H &= 0 \end{aligned}\right\} \quad (23)$$

The vertical disturbance velocity on the body axis due to body angle of attack can be obtained from figure 10 which was prepared by use of equation (23).

Some Additional Considerations

In estimating the errors in flow angularity that would result with an angle-measuring pickup located ahead of a body nose, consideration should be given not only to the effects of the fuselage but also to the effects of the supporting boom on which the pickup will be mounted and to the effects of the airplane wing.

Effects of supporting boom.- In some instances angle-measuring vanes are attached to fuselage nose booms as indicated in figure 11. In such cases, if the boom is at an angle of attack, the component of stream velocity normal to the axis of the boom will cause additional errors in the measured values of angle of attack and sideslip. For small angles of attack, the velocity components in planes normal to the axis of the boom are so small that incompressible-flow theory may be used. If the boom is regarded as a circular cylinder of infinite length at an angle of attack, the radial velocity component at any point is $-V\left(1 - \frac{a^2}{r^2}\right)\cos\theta\sin\alpha$ and the tangential velocity component is $V\left(1 + \frac{a^2}{r^2}\right)\sin\theta\sin\alpha$ (see ref. 3). The sum of these components in the direction of $V\sin\alpha$ is

$$\left[\left(1 - \frac{a^2}{r^2}\right)\cos 2\theta\right] V\sin\alpha$$

The disturbance velocity v_V is

$$v_V = \left[\left(1 - \frac{a^2}{r^2}\right)\cos 2\theta\right] V\sin\alpha - V\sin\alpha \quad (24)$$

and therefore for small angles of attack

$$\frac{v_V}{V} = \Delta\alpha = -\frac{\alpha}{(r/a)^2}\cos 2\theta \tag{25}$$

Similarly,

$$\frac{v_H}{V} = -\Delta\beta = \frac{\alpha}{(r/a)^2}\sin 2\theta \tag{26}$$

The quantities

$$\left.\begin{aligned} \frac{v_V}{V}\frac{(r/a)^2}{\alpha} &= \frac{\Delta\alpha}{\alpha}\left(\frac{r}{a}\right)^2 \\ \frac{v_H}{V}\frac{(r/a)^2}{\alpha} &= -\frac{\Delta\beta}{\alpha}\left(\frac{r}{a}\right)^2 \end{aligned}\right\} \tag{27}$$

are plotted as a function of θ in figure 12. The effect of the supporting boom in the case of sideslip can be calculated by considering the angle of sideslip to be an angle of attack and rotating the origin of θ accordingly. If the vane is located at a position other than $\theta = 0^\circ$, 90°, or 180°, the disturbance velocities will be such that the angle-of-attack indication is affected by sideslip and vice versa.

Effects of wing.- As an approximate means for estimating the effect of the wing on the flow inclination, the simple horseshoe vortex system of figure 13 may be used. The bound vortex may be considered to lie on the quarter-chord line of the wing. In reference 4 expressions are given for the contributions to the induced velocity components, in subsonic flow, due to the bound vortex and due to each trailing vortex of such a horseshoe vortex system. If the angle-of-attack vane is considered to lie on the X'-axis, that is, in the chord plane extended and in the plane of symmetry as indicated in figure 13, the effect of the horseshoe vortex system is to induce an upflow velocity at the vane which can be expressed by the relation

$$w_W = -\frac{\Gamma}{2\pi s}\left[1 + \frac{\sqrt{(x'/Bs)^2 + 1}}{x'/Bs}\right] \tag{28}$$

which is the sum of the upflow components of velocity induced by each segment of the horseshoe vortex.

The circulation Γ is related to the lift of the wing by

$$2s\rho V\Gamma = \frac{1}{2}\rho V^2 \frac{4s^2}{A} C_{L_\alpha}\alpha = \text{Lift}$$

and, by using the lifting-line value for the lift-curve slope $\left(C_{L_\alpha} = \frac{2\pi A}{BA + 2}\right)$, the circulation may be expressed as

$$\Gamma = 2\pi sV \frac{\alpha}{BA + 2}$$

Equation (28) may then be written as

$$\frac{w_W}{V} = -\frac{\alpha}{BA + 2}\left[1 + \frac{\sqrt{(x'/Bs)^2 + 1}}{x'/Bs}\right] \tag{29}$$

The error in the inclination of an angle-of-attack vane resulting from the induced upflow of the wing may be written as

$$\frac{\Delta\alpha}{\alpha} = -\frac{1}{BA + 2}\left[1 + \frac{\sqrt{(x'/Bs)^2 + 1}}{x'/Bs}\right] \tag{30}$$

which has been plotted in figure 14. Note that the coordinate x' appearing in this relation is the distance from the quarter-chord line. As an example, suppose that an angle-of-attack vane is located 1 semispan ahead of the quarter-chord line of a wing of aspect ratio 6 and it is required to find the error in angle of attack introduced by the wing at a Mach number of 0.6. From figure 14 at a value of x'/Bs of -1.25, there is found a value of $\frac{\Delta\alpha}{\alpha}(BA + 2)$ equal to 0.28. Hence, under these conditions $\frac{\Delta\alpha}{\alpha} = 0.041$. At 1 semispan ahead of the center of the quarter-chord line, which is rather near the wing for most nose-boom installations, the error in angle of attack introduced by the wing is about 4 percent of the true value.

EXPERIMENT

Some experimental data were obtained from tests made in the 6- by 6-foot test section of the Langley stability tunnel. The body tested was a parabolic-arc body of revolution such as those for which the formulas were derived. The body was 42 inches long and had a maximum diameter of 7 inches (fineness ratio of 6). A 3/8-inch-diameter combination pitot-static and angle-head tube was used for the measurements of static pressure, total pressure, and flow angularity.

Measurements were made for different angles of attack along the body axis and along lines parallel to the axis located at various distances above, below, and to one side of the body axis. Tests were made both with and without the body for identical location of the pitot-static tube and were carried out at an impact pressure of approximately 65 pounds per square foot which corresponded to a Mach number of about 0.21.

In reducing the data, the effects of local angularity on the static-pressure measurements as well as the effects of displacement of the static-pressure orifices relative to the total-pressure orifice were taken into account.

The experimental data are presented in figures 15 to 24 together with the appropriate theoretical calculations for purposes of comparison.

DISCUSSION AND COMPARISON OF THEORY WITH EXPERIMENT

Effects of Thickness

Pressure coefficient.- The incremental static-pressure coefficient to be expected ahead of the body nose at zero angle of attack may be estimated from figure 3.

The static pressure is seen to be a maximum at points on the body axis and to decrease with distance away from the axis. As a matter of interest, equation (10) shows that the static pressure on the axis is independent of Mach number.

As an example of the use of figure 3, suppose that the location of the static orifices on the axis is taken at 1 maximum fuselage diameter ahead of the nose of a fuselage with a fineness ratio of 6. The value of x at 1 diameter ahead of this fuselage nose is equal to -1.33. At this value of x, the value of $F^2\left(\frac{\Delta p}{q}\right)_1$ is found to be 0.88 so that $\left(\frac{\Delta p}{q}\right)_1$ is about 0.024. In order to obtain an incremental pressure

coefficient of less than 0.01 for this fuselage, it is necessary to locate orifices at a value of x more negative than -1.64 or at a distance greater than 1.92 maximum diameters ahead of the fuselage nose.

In figure 15 is shown a comparison of the calculated and measured values of $\left(\frac{\Delta p}{q}\right)_1$ for the parabolic-arc body of fineness ratio 6 at a Mach number of 0.21. In general, the agreement shown in figure 15 is good, although the theory appears to overestimate slightly the value of $\left(\frac{\Delta p}{q}\right)_1$.

Flow inclination.- The inclination of the flow, with respect to the direction of the stream, to be expected ahead of a fuselage due to body thickness may be estimated from figure 4. The quantity $\frac{v_1}{V}\frac{F^2}{B}$ is shown plotted against x for several values of Br. If v_1/V is multiplied by $\cos\theta$, there results the correction to be added to the indication of an angle-of-attack vane located at the point (x,r,θ) (see fig. 1). The correction to be made to the indications of an angle-of-sideslip vane can be obtained from figure 4 by multiplying v_1/V by $\sin\theta$ with proper regard to sign. For vanes located on the axis of the body, no correction is necessary at zero angle of attack and sideslip.

The calculated and measured changes in flow inclination due to body thickness are shown to be in good agreement in figure 16.

Effects of Angle of Attack

Pressure coefficient.- The theoretical incremental static-pressure coefficient due to angle of attack $\left(\frac{\Delta p}{q}\right)_2$ may be obtained from figure 4. This is the pressure coefficient obtained by using equation (14) (see section entitled "Application of Theory"). The static-pressure-coefficient increment ahead of the fuselage nose at angles of attack is, of course, $\left(\frac{\Delta p}{q}\right)_1 + \left(\frac{\Delta p}{q}\right)_2$.

The calculations show that at points ahead of the body on the extended axis of the body the static-pressure increment does not vary with angle of attack but remains always at the value for zero angle of attack. (See fig. 17.) The measured points in figure 17 are from three test runs: a positive angle of attack, a negative angle of attack, and a positive angle of sideslip. (For Br = 0 the results should, of course, be identical.) The scatter, especially that at higher angles, may be attributed to

unsteady flow, a possible shift of stagnation point, and to a fairly large pressure gradient near the body nose. Although the fact that the theory is strictly valid only for small angles of attack is fully realized, comparisons between theory and experiment at angles of attack as high as 30° are presented in figures 17 to 20. These comparisons show that close to the body nose the theory adequately predicts the pressure increment at low angles of attack but not at the higher angles. As the distance from the nose increases, the agreement between theory and experiment improves for all angles of attack.

The effect of angle of sideslip on the pressure coefficient can be obtained from figure 4 by considering the angle of sideslip to be an angle of attack with proper regard to sign. In the case of a combined angle of attack and sideslip, two methods of obtaining pressures are possible which lead to identical results. The values of $\left(\frac{\Delta p}{q}\right)_2$ due to separate angles of attack and of sideslip can be computed and added algebraically or the resultant angle may be computed and the corresponding value of $\left(\frac{\Delta p}{q}\right)_2$ may be found.

Flow inclination.- For vanes located on the axis ahead of the body, the flow inclination due to angle of attack $\frac{v_V}{V} \approx \Delta\alpha$ may be found from figure 10 in which the quantity $\frac{v_V}{V}\frac{F^2}{B^2\alpha}$ at $Br = 0$ is shown plotted against x. The quantity $\frac{v_V}{V}\frac{F^2}{B^2\alpha}$ can be expressed for small angles as $\frac{F^2}{B^2}\frac{\Delta\alpha}{\alpha}$ where $\Delta\alpha$ is to be considered as the increment in angle of attack indicated by a vane. If α_i is the angle of attack indicated by a vane, the correct angle of attack is given by the relation

$$\alpha = \frac{\alpha_i}{1 + \frac{\Delta\alpha}{\alpha}}$$

For vanes located off the axis, the incremental angle of attack may be calculated from equation (15) which shows that for small angles

$$\Delta\alpha \approx \frac{v_V}{V} = \frac{w_2}{V}\sin\theta - \frac{v_2}{V}\cos\theta$$

The increment in angle of sideslip is shown by equation (16) to be

$$\Delta\beta \approx \frac{v_H}{V} = \frac{w_2}{V} \cos\theta + \frac{v_2}{V} \sin\theta$$

The values of v_2/V and w_2/V which appear in these equations may be estimated from figures 8 and 9, respectively.

As an example, suppose that an angle-of-attack vane is located on the axis at 1 maximum diameter ahead of the nose of a fuselage of fineness ratio 6 and it is required to find the increment in the indication of the vane at a Mach number of 0.6. At a value of $x = -1.33$, figure 10 shows that

$$\frac{F^2}{B^2\alpha} \frac{v_V}{V} = 0.44$$

Then

$$\frac{\Delta\alpha}{\alpha} = \frac{1}{\alpha} \frac{v_V}{V} = 0.44 \frac{B^2}{F^2} = 0.0078$$

The increment in angle of attack is, then, less than 1 percent of the true value.

A comparison of the calculated and measured change in flow inclination on the axis due to inclination of the test body is shown in figure 21. The measured results in the figure show a considerable scatter especially at high angles. The measured points are from three test runs: a positive angle of attack, a negative angle of attack, and a positive angle of sideslip. (For $Br = 0$, the results should, of course, be identical.) The scatter in experimental results at the higher angles may be attributed in part to unsteady flow about the body at these high angles of attack, to a possible shift in stagnation point, and to a fairly large gradient of airstream angularity near the body nose. In general, the measured results show a somewhat greater induced angle on the axis than that predicted by the calculations.

For positions off the axis, the angles induced by the body are shown (figs. 22 to 24) to be fairly small and to be estimated fairly well by the calculations. The maximum differences between measured and calculated values occur close to the nose of the body and at higher angles of attack. At distances greater than 1/2 diameter ahead of a body of fineness ratio 6 and at angles less than 20°, the simplified calculations used herein adequately predict the local angularity due to the presence of the body.

CONCLUDING REMARKS

Subsonic linearized theory has been used to derive approximate expressions for the incremental pressure coefficient and flow inclination ahead of slender parabolic-arc bodies of revolution. Charts have been presented from which deviations from free-stream values in the indicated values of static pressure, angle of attack, and angle of sideslip can be estimated for any position so that suitable positions for locating static-pressure orifices and angle-of-attack and angle-of-sideslip vanes can readily be selected. Comparisons between calculated values and those measured at a Mach number of 0.21 for a body of fineness ratio 6 show that for distances greater than 1/2 body diameter in front of the body nose and for angles of attack less than 20° the approximate theory used herein is adequate for predicting the best location for static-pressure and angle-measuring pickups.

Calculations indicate that the angle-of-attack deviation introduced by the wing may be large for some configurations and should be considered in determining a suitable location for an angle-measuring pickup.

Langley Aeronautical Laboratory,
National Advisory Committee for Aeronautics,
Langley Field, Va., April 30, 1954.

REFERENCES

1. Laitone, E. V.: The Subsonic Flow About a Body of Revolution. Quarterly Appl. Math., vol. V, no. 2, July 1947, pp. 227-231.

2. Laitone, E. V.: The Linearized Subsonic and Supersonic Flow About Inclined Slender Bodies of Revolution. Jour. Aero. Sci., vol. 14, no. 11, Nov. 1947, pp. 631-642.

3. Glauert, H.: The Elements of Aerofoil and Airscrew Theory. Second ed., Cambridge Univ. Press, 1947. (Reprinted 1948.)

4. Tsien, Hsue-Shen, and Lees, Lester: The Glauert-Prandtl Approximation for Subsonic Flows of a Compressible Fluid. Jour. Aero. Sci., vol. 12, no. 2, Apr. 1945, pp. 173-187, 202.

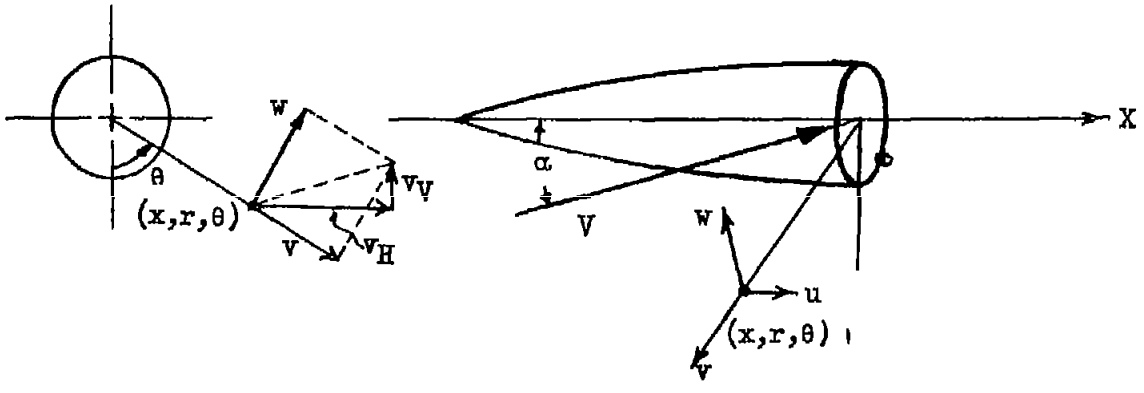

(a) Front view. (b) Side view.

Figure 1.- Cylindrical coordinate system.

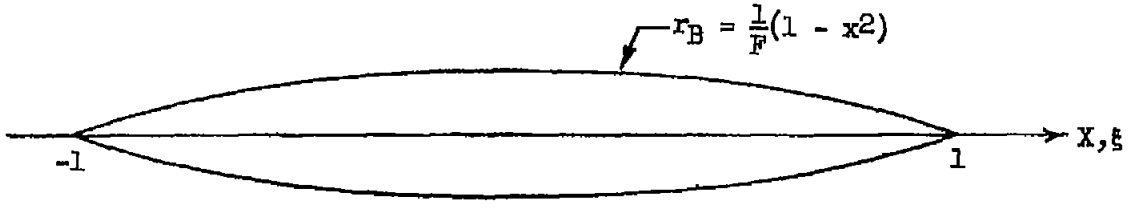

Figure 2.- Parabolic-arc body of revolution.

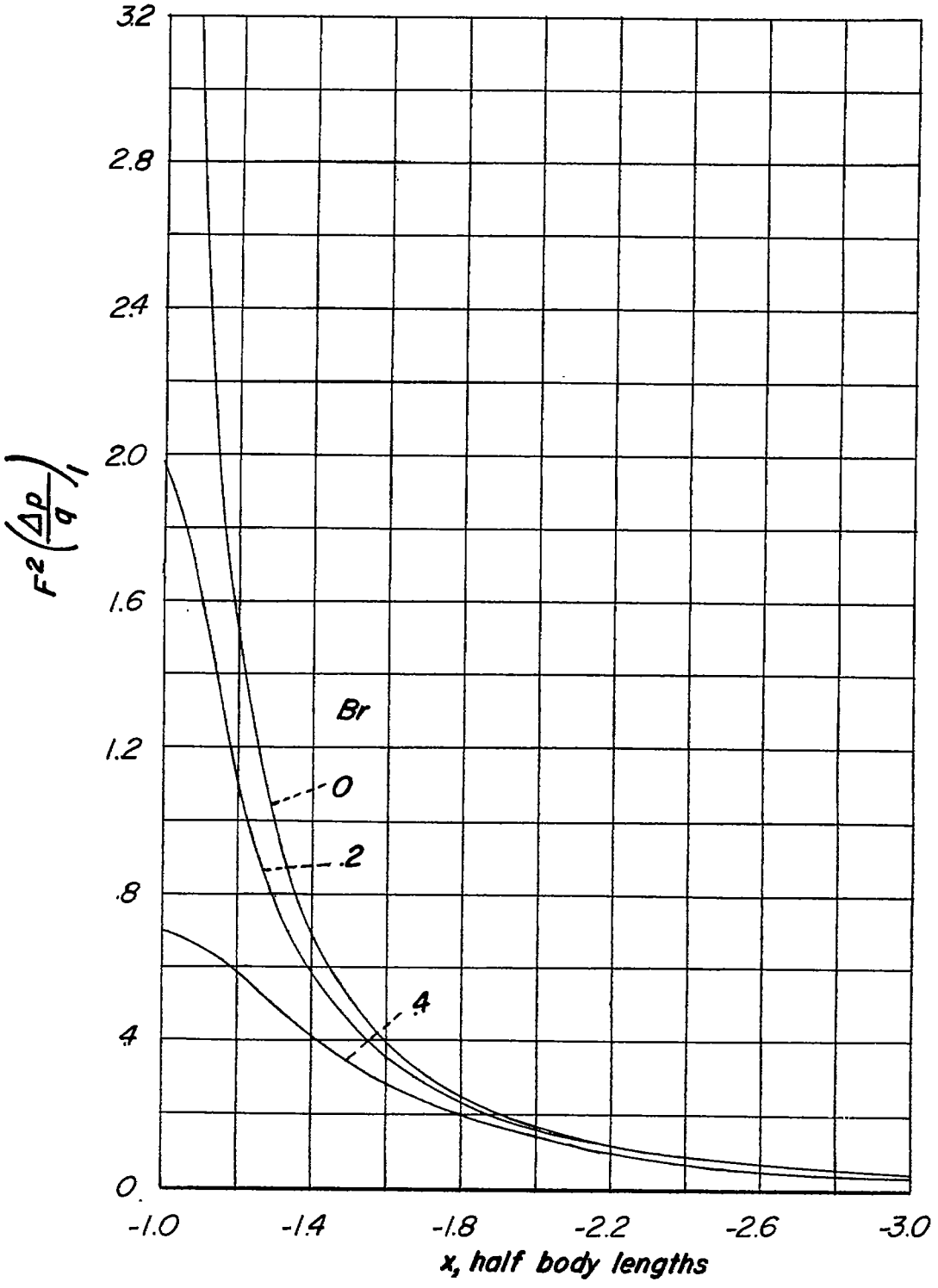

Figure 3.- Incremental pressure coefficient ahead of a parabolic-arc body of revolution at zero angle of attack. Equation (9).

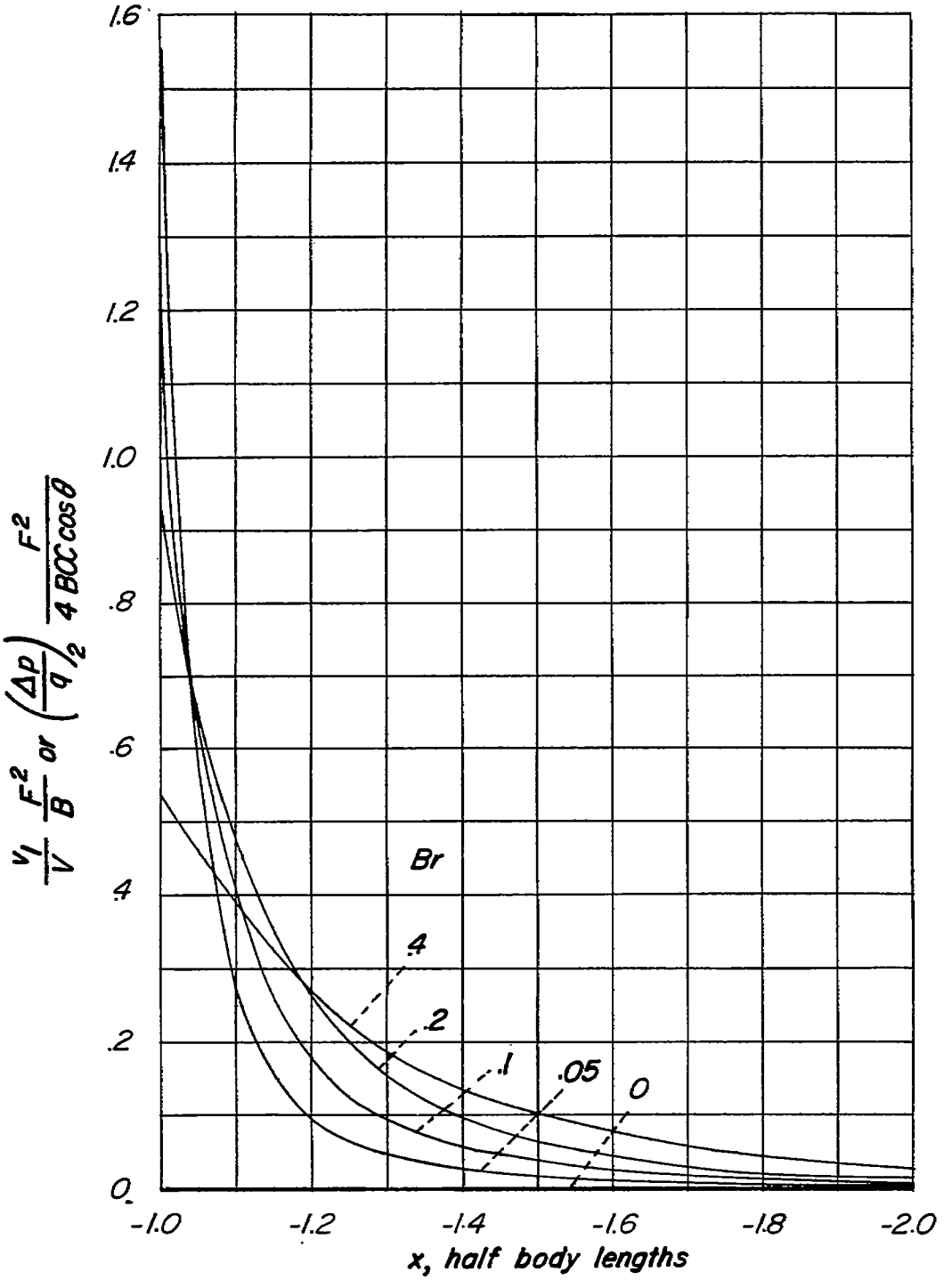

Figure 4.- Flow inclination at zero angle of attack and incremental pressure coefficient ahead of parabolic-arc body of revolution due to angle of attack. Equations (11) and (14).

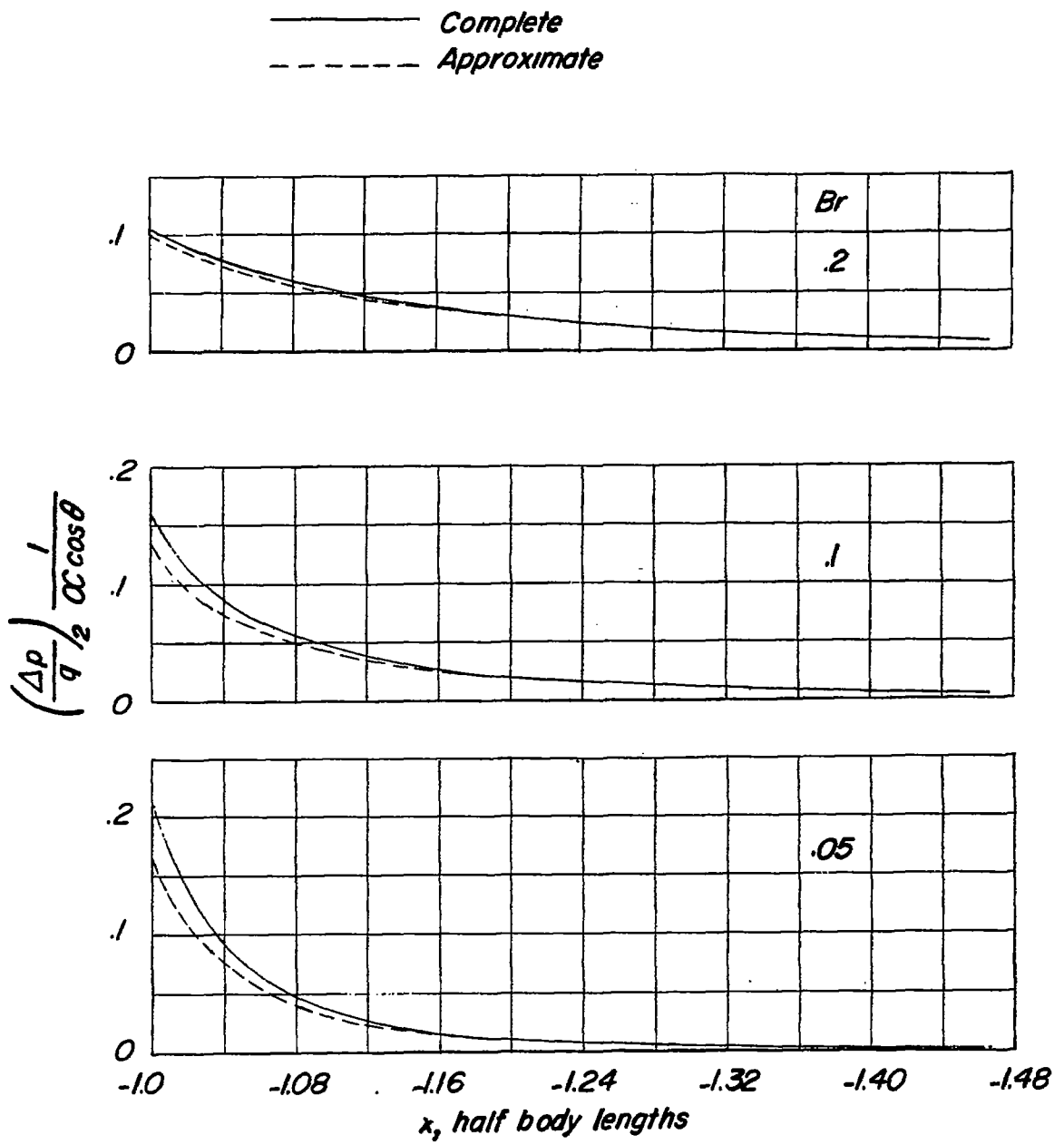

Figure 5.- Comparison of the incremental pressure coefficient due to body angle of attack determined by an approximate solution of equation (13) with that determined by the complete solution of the equation. F = 6; M = 0.21.

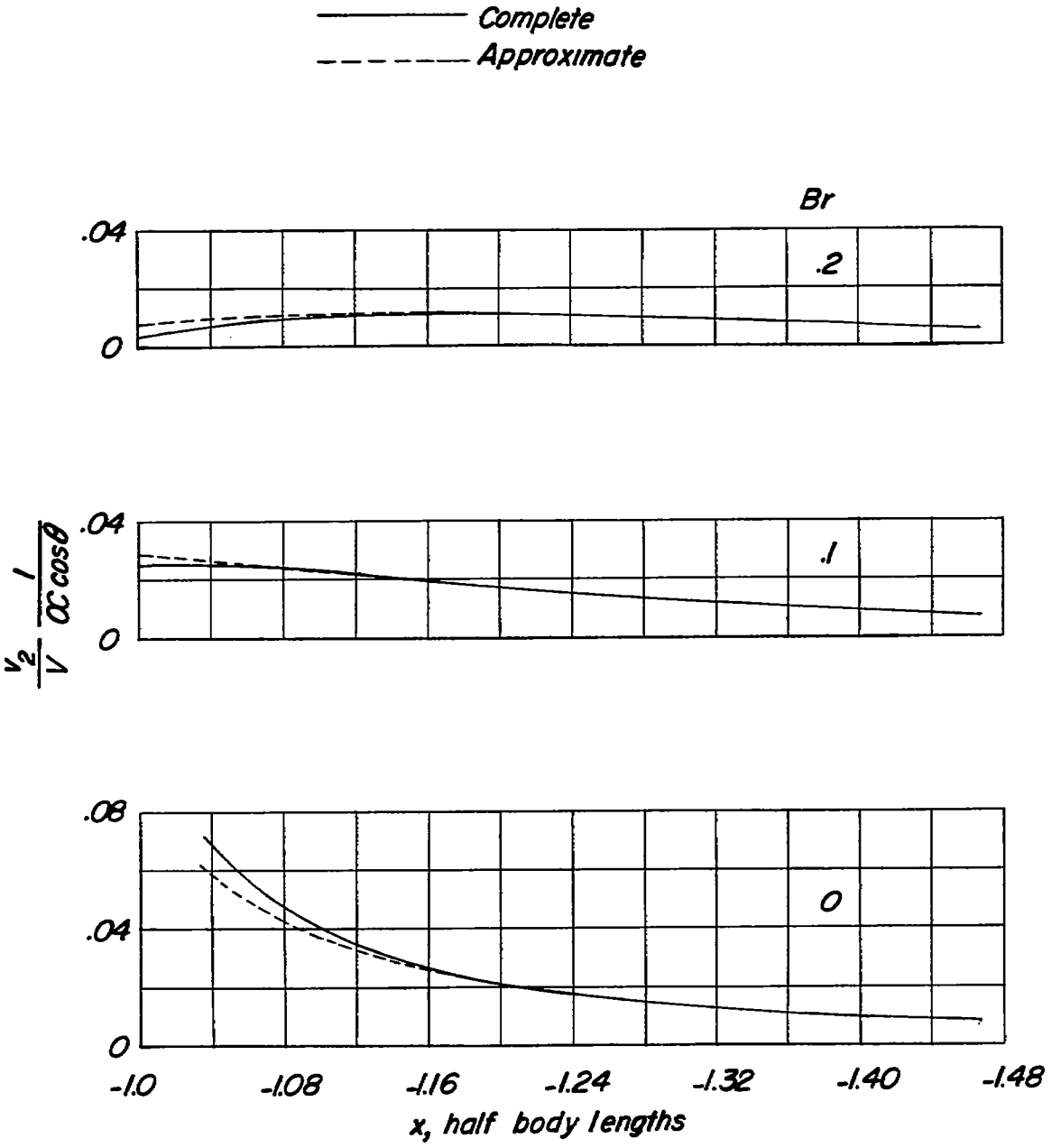

Figure 6.- Comparison of the radial disturbance velocity component due to angle of attack determined by an approximate solution of equation (17) with that determined by the complete solution. F = 6; M = 0.21.

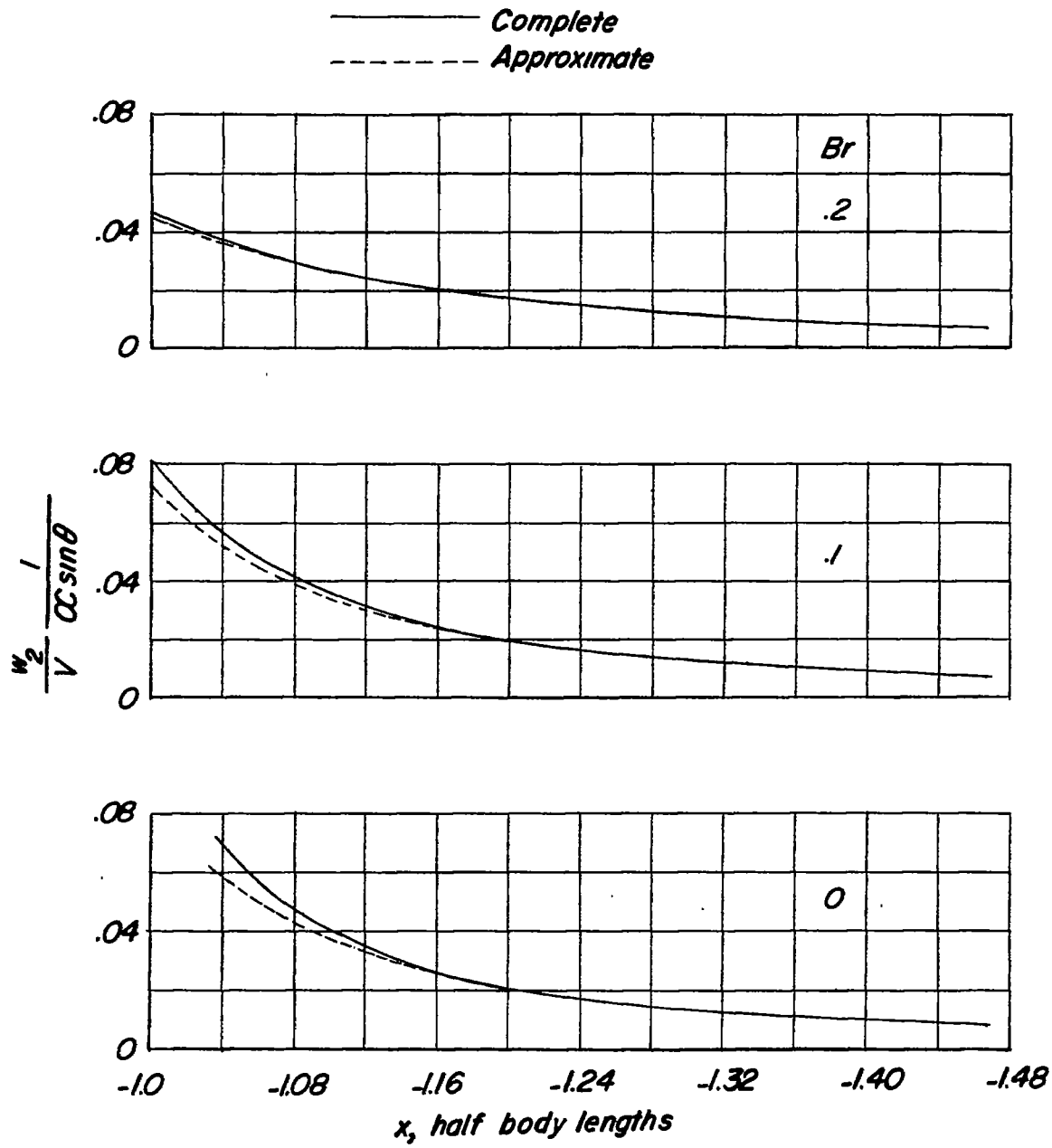

Figure 7.- Comparison of the tangential disturbance velocity component due to angle of attack determined by an approximate solution of equation (18) with that determined by the complete solution. F = 6; M = 0.21.

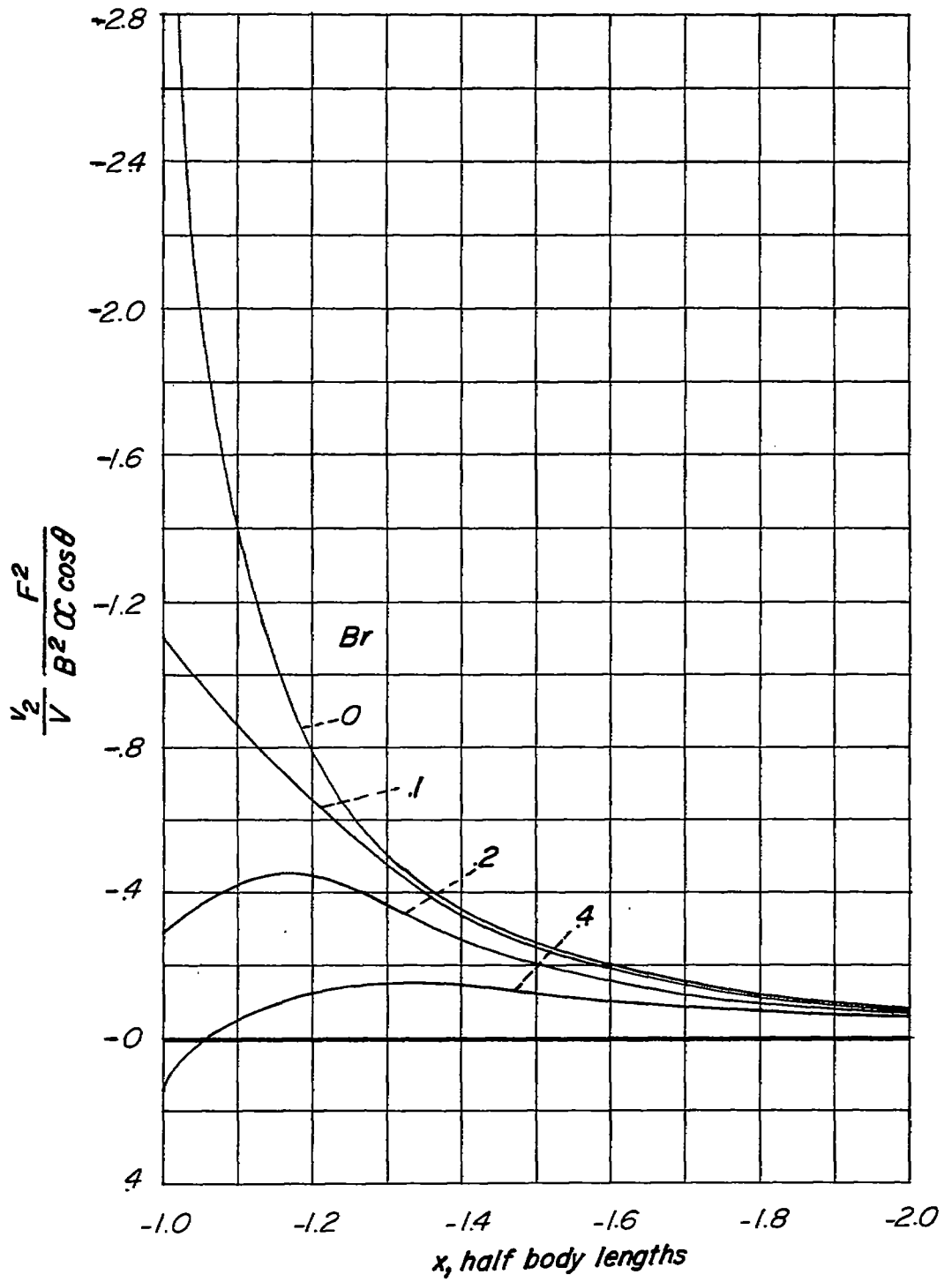

Figure 8.- Radial disturbance velocity component ahead of a parabolic-arc body of revolution due to angle of attack. Equation (19).

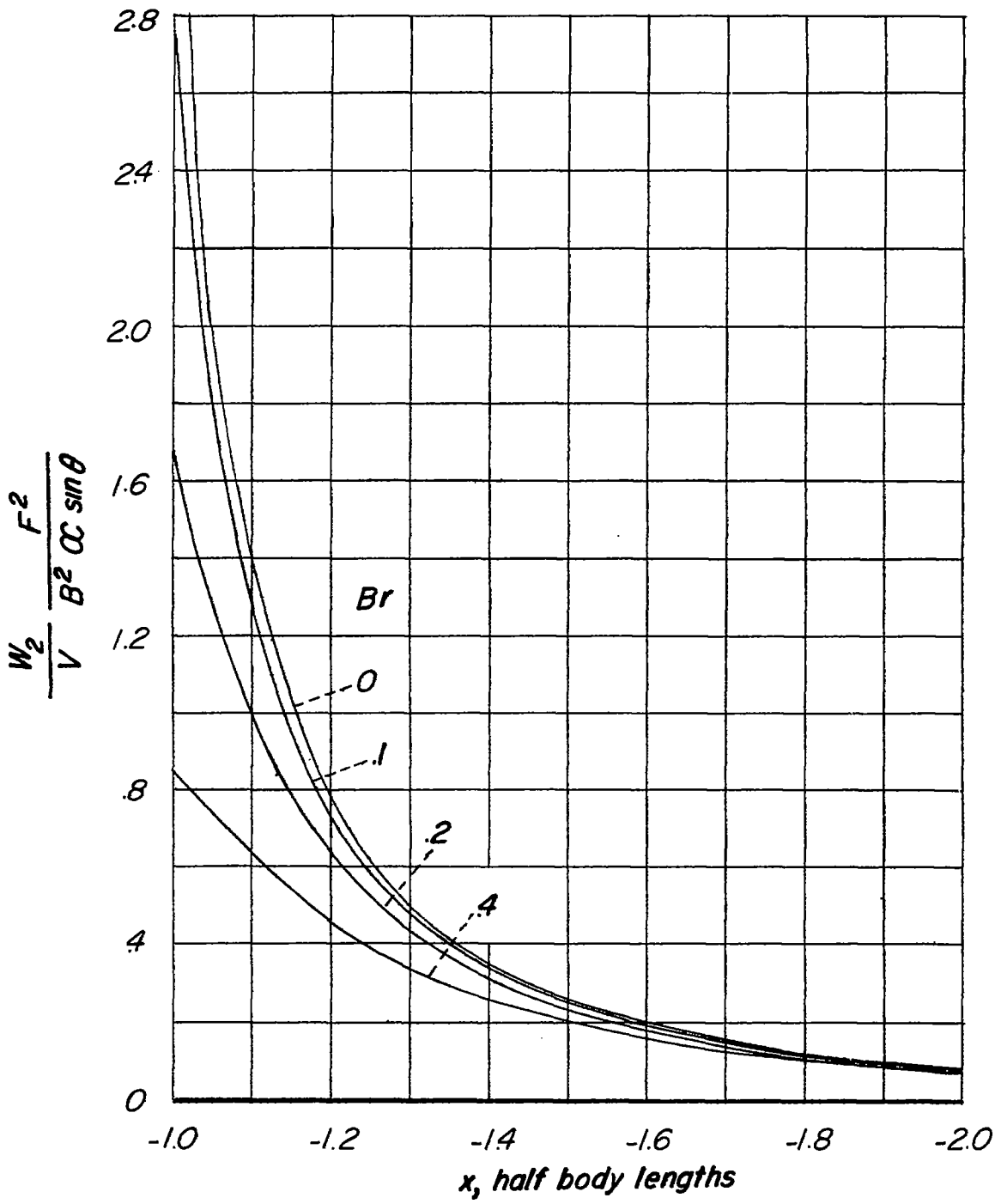

Figure 9.- Tangential disturbance velocity component ahead of parabolic-arc body of revolution due to angle of attack. Equation (20).

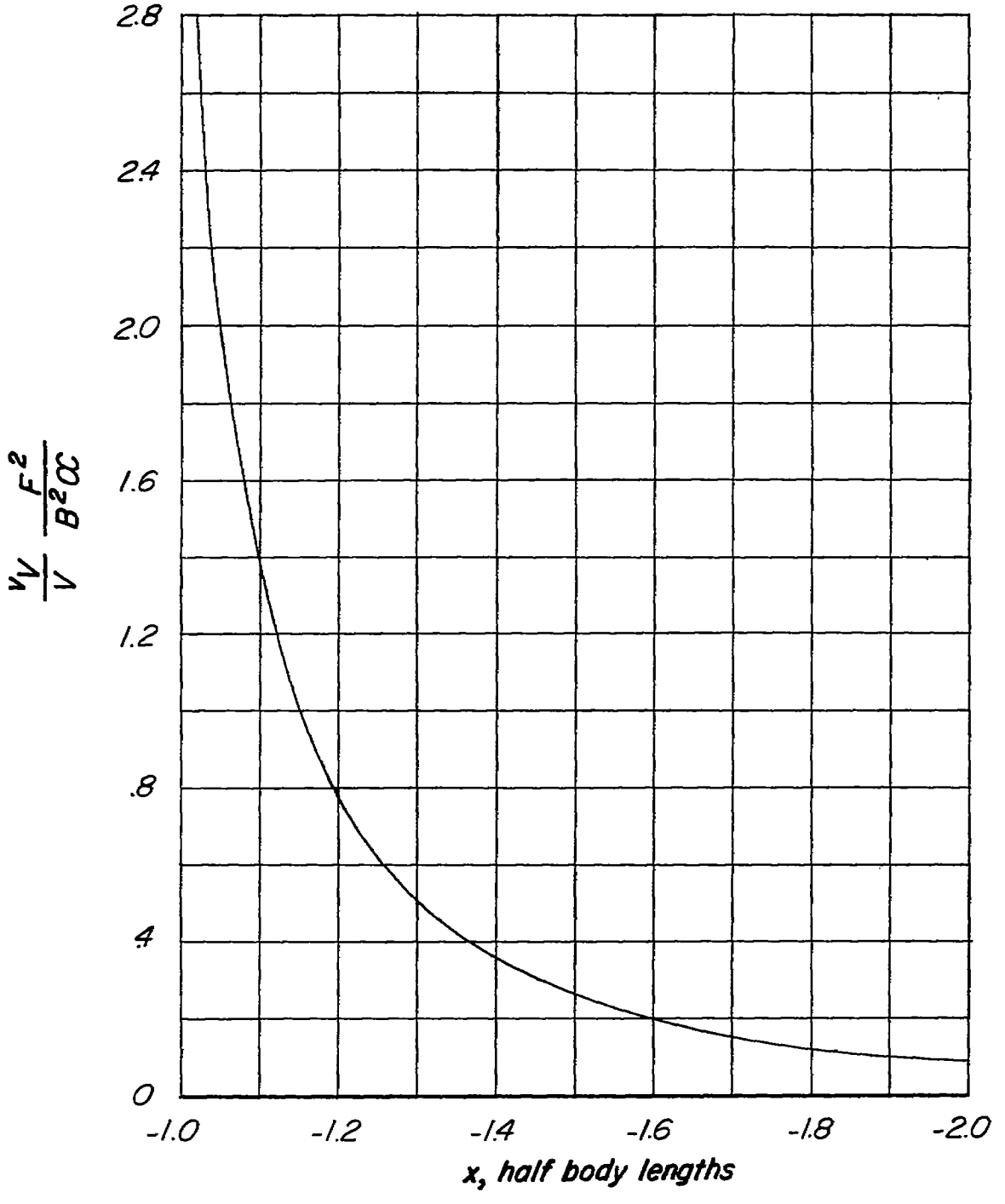

Figure 10.- Flow inclination on the body axis ahead of parabolic-arc body of revolution due to angle of attack. Equation (23).

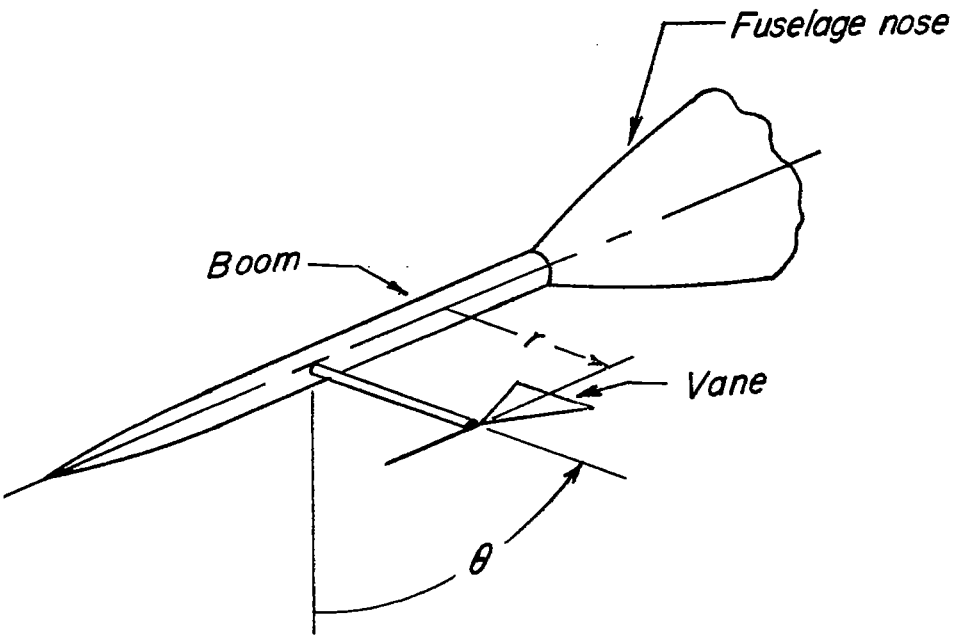

Figure 11.- Example of support for angle-of-attack vane.

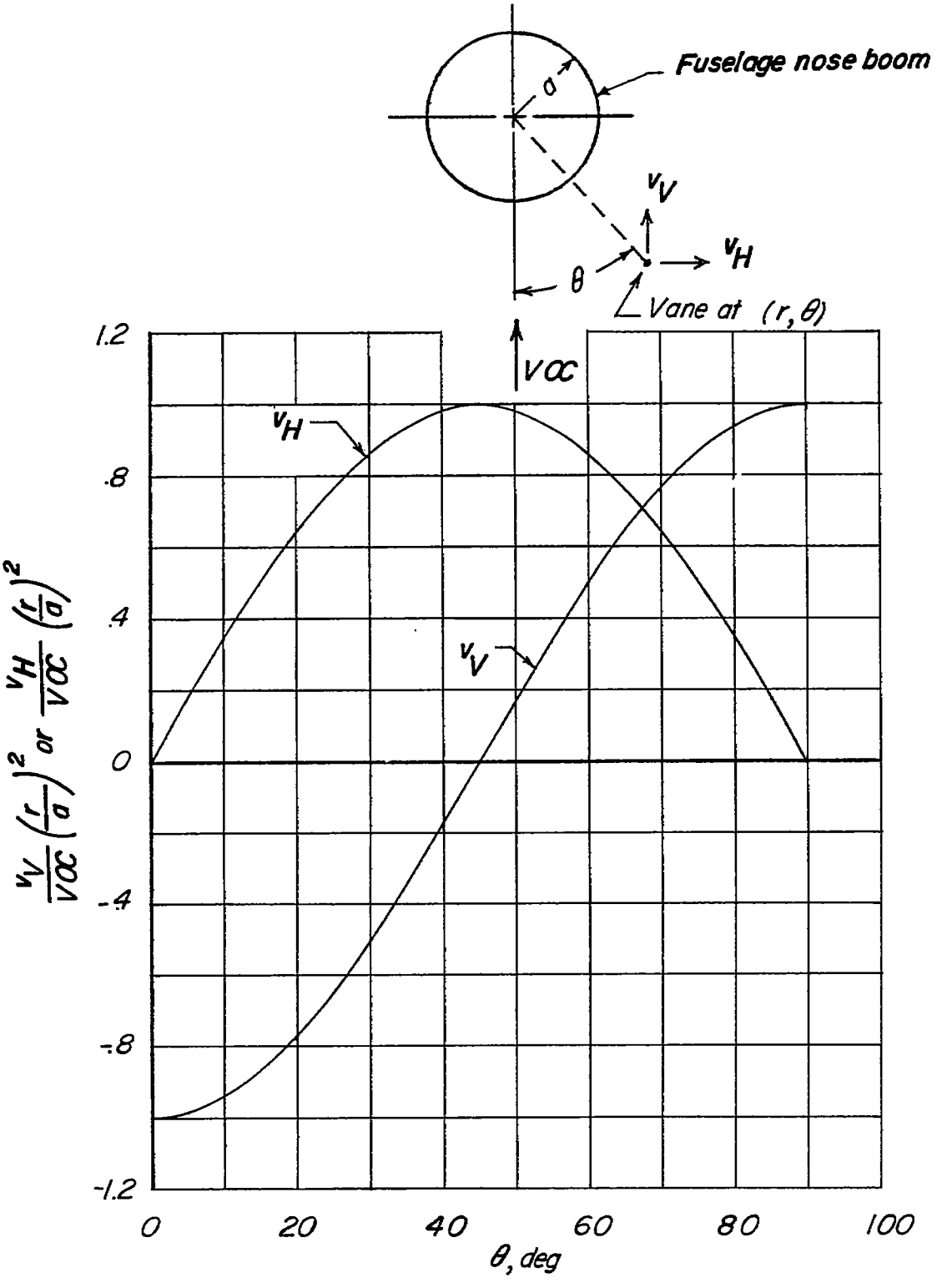

Figure 12.- Flow inclination caused by support boom for angle-of-attack vane shown in figure 11.

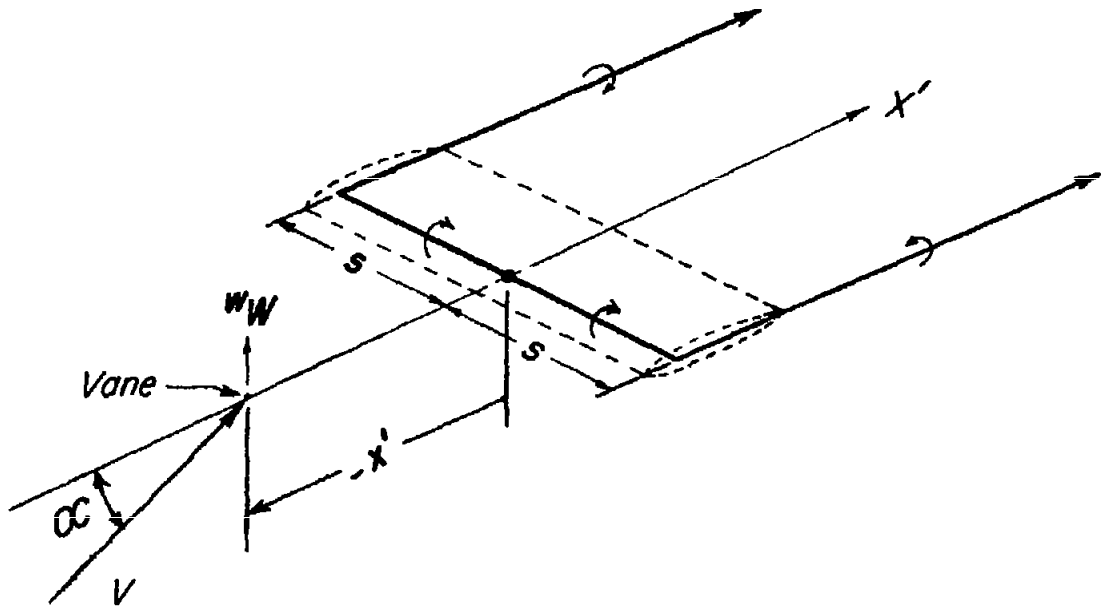

Figure 13.- Horseshoe vortex system used in the calculation of the effect of wing lift on the indication of an angle-of-attack vane.

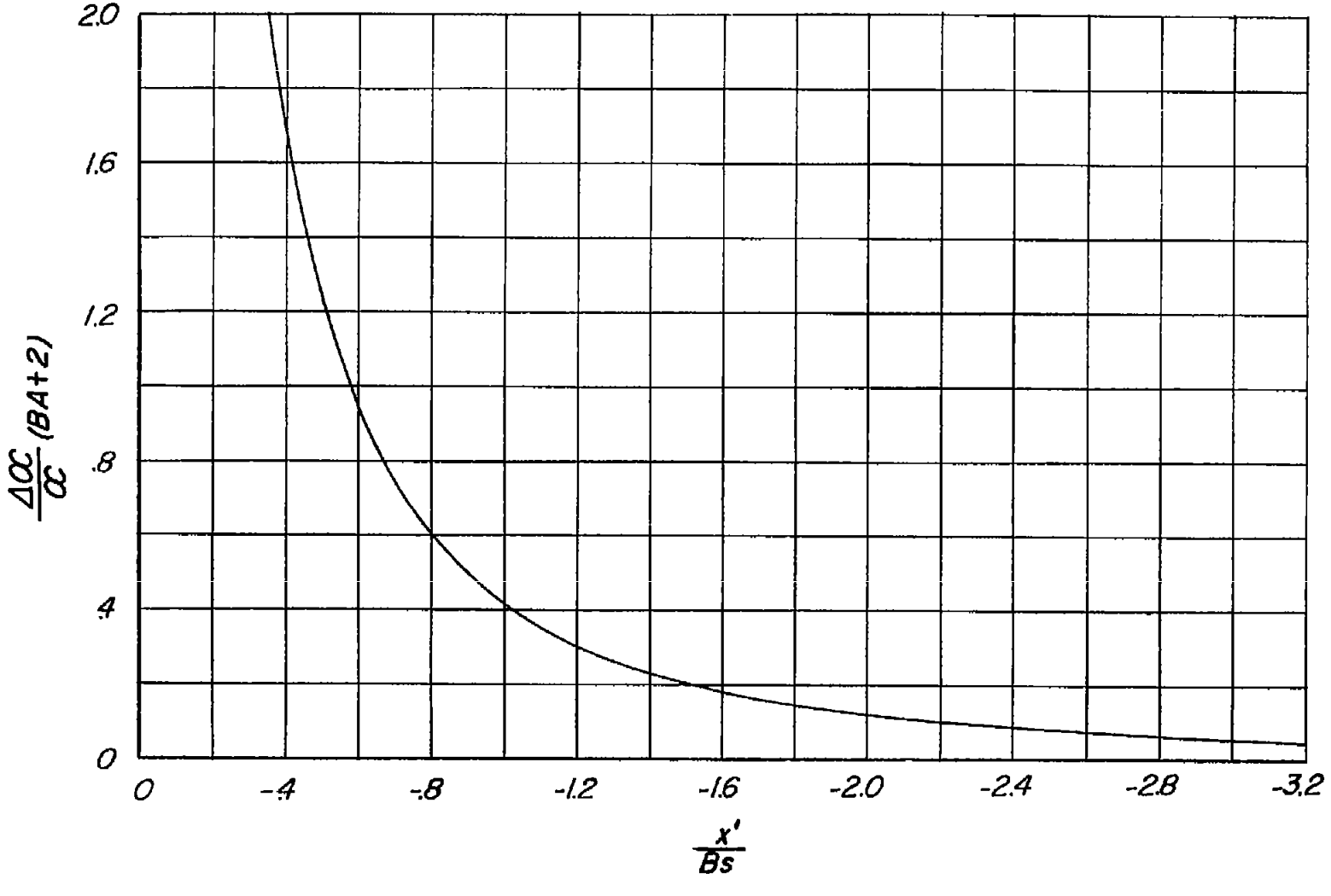

Figure 14.- Effect of lifting wing on the indication of an angle-of-attack vane mounted as shown in figure 13.

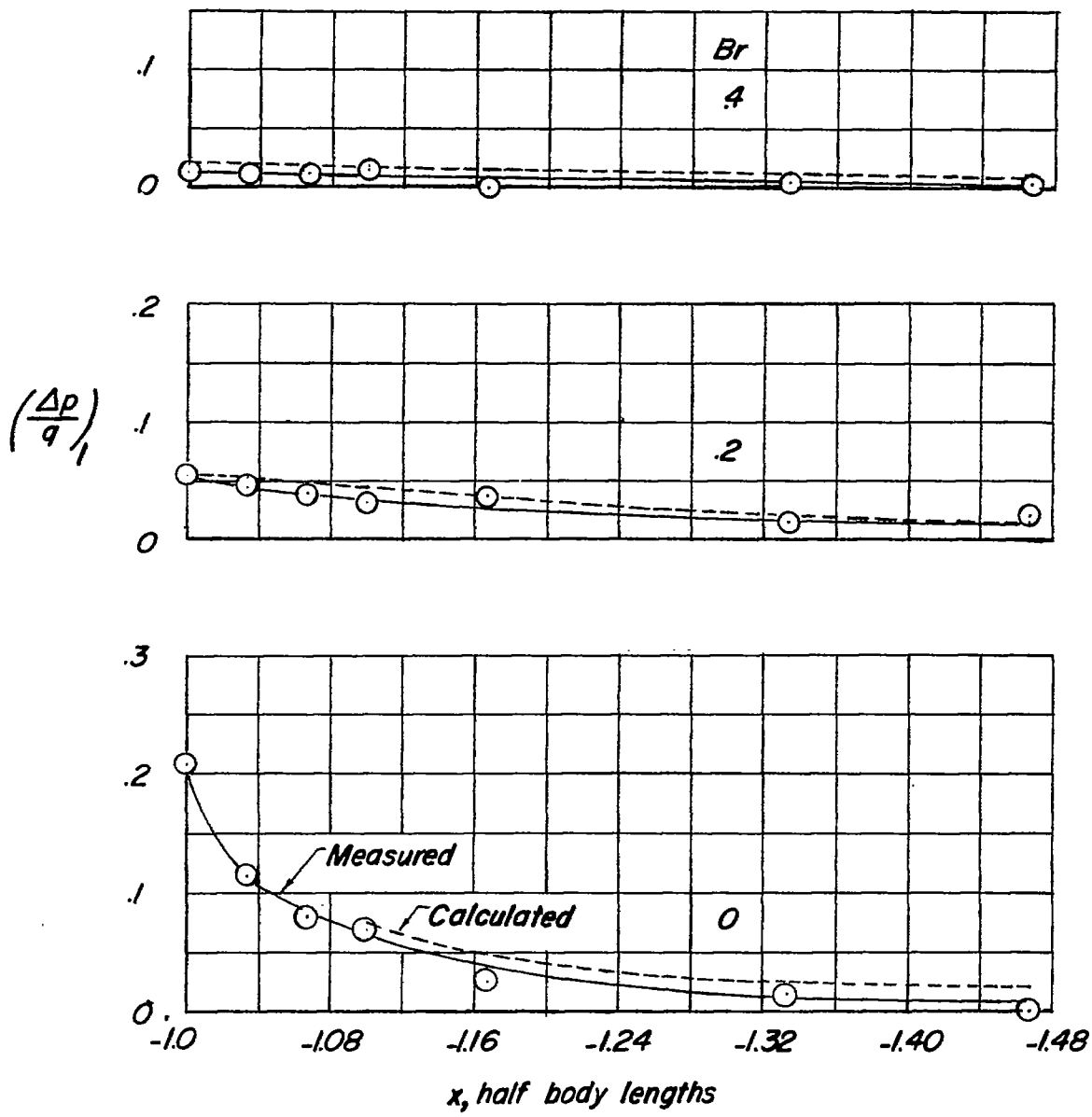

Figure 15.- Comparison of the calculated and measured incremental pressure coefficient ahead of a parabolic-arc body of revolution at zero angle of attack. F = 6; M = 0.21.

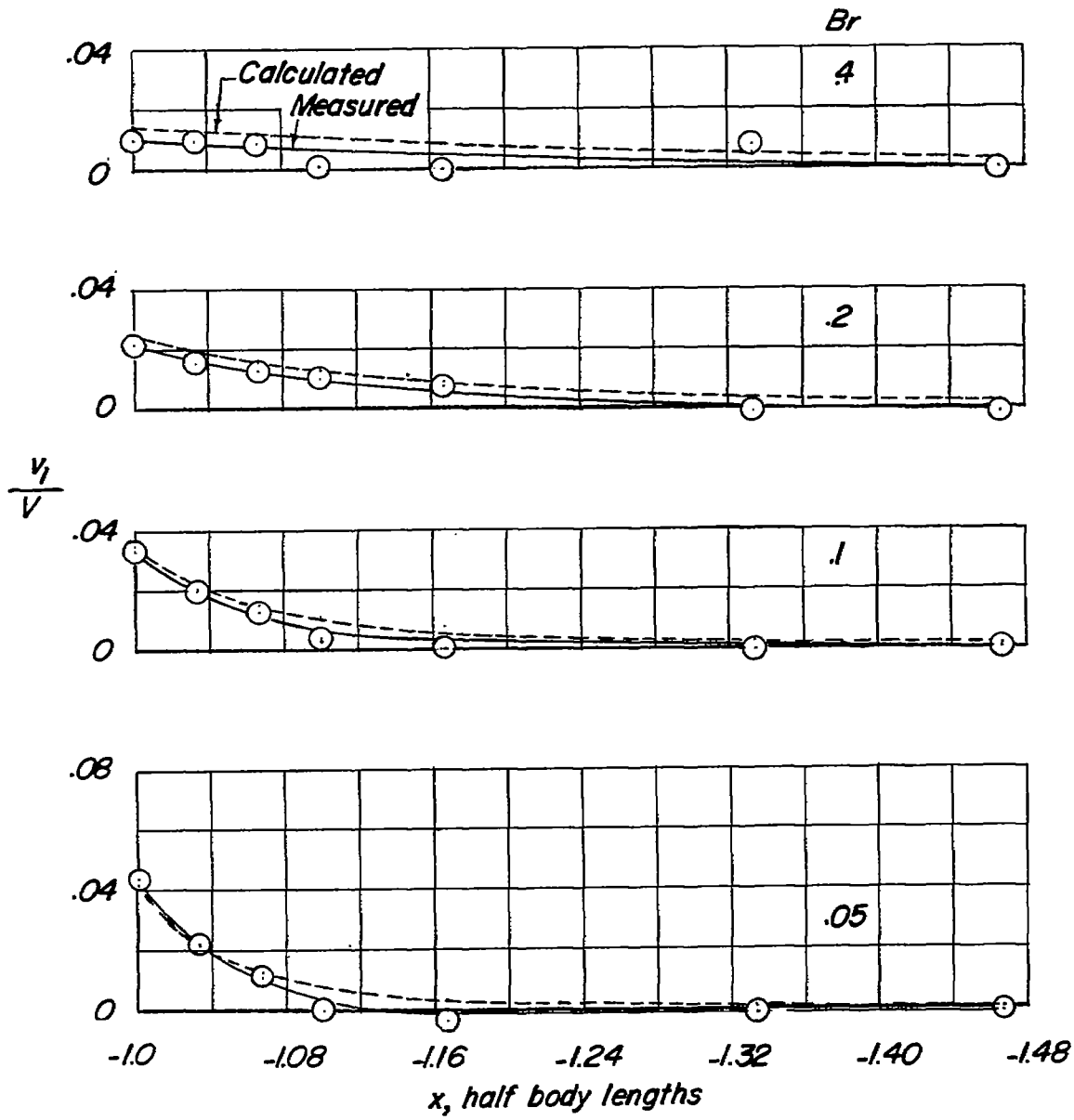

Figure 16.- Comparison of the calculated and measured change in flow inclination ahead of a parabolic-arc body of revolution at zero angle of attack. F = 6; M = 0.21.

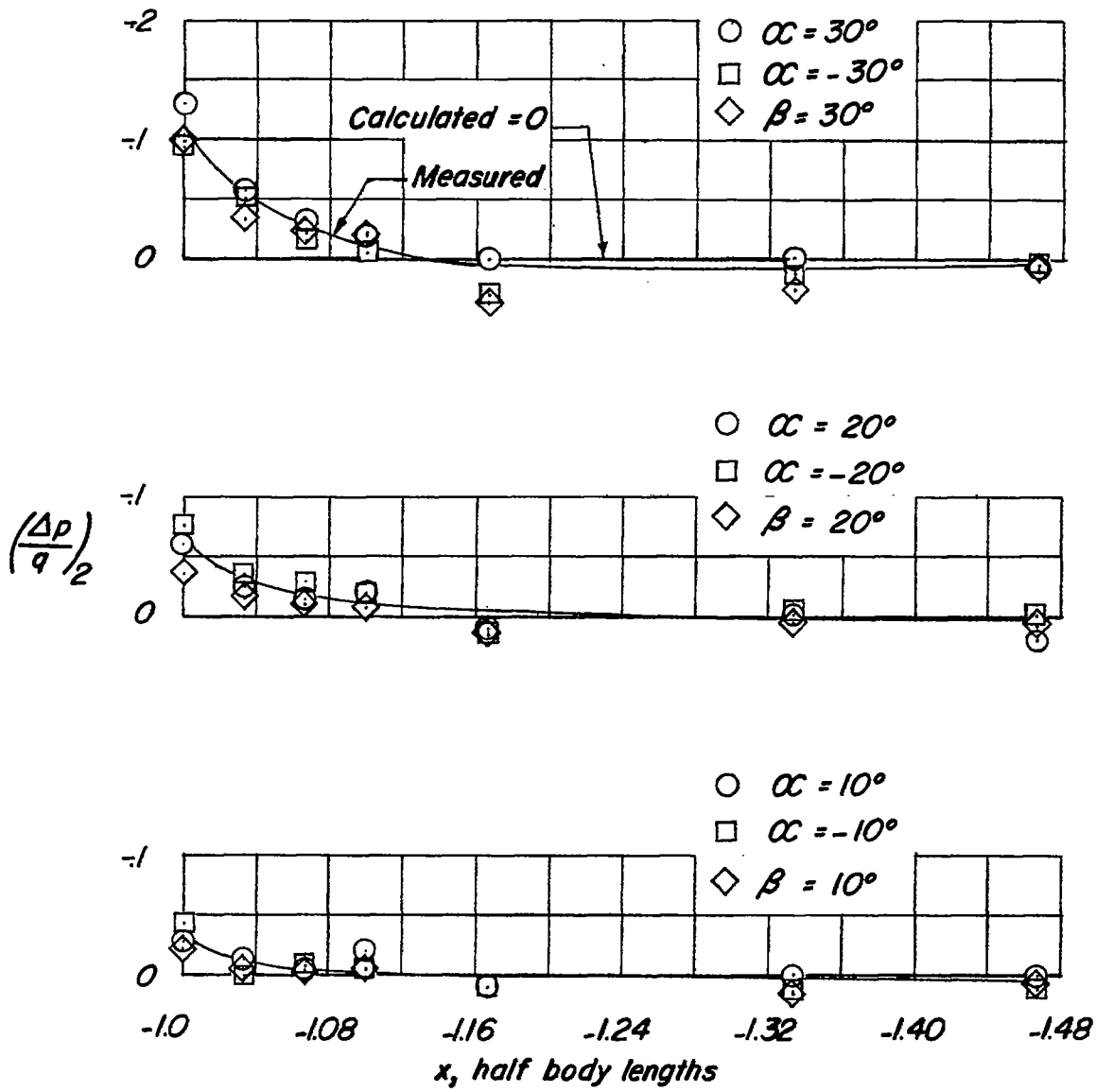

Figure 17.- Comparison of the calculated and measured incremental pressure coefficient on the body axis ahead of a parabolic-arc body of revolution due to inclination of body. F = 6; M = 0.21.

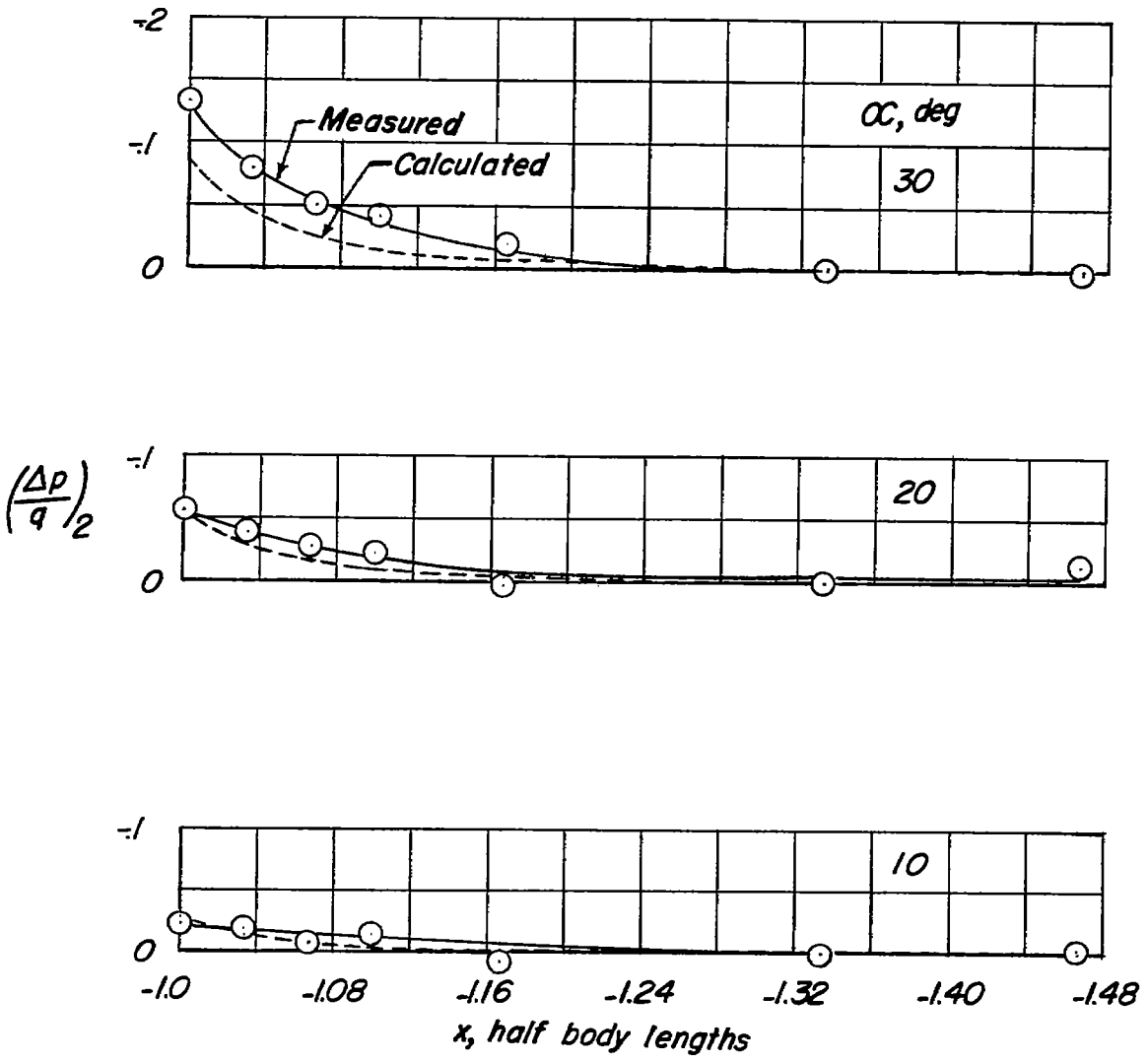

(a) Br = 0.05; $\theta = 180^{\circ}$.

Figure 18.- Comparison of the calculated and measured incremental pressure coefficient at $\theta = 180^{\circ}$ ahead of a parabolic-arc body of revolution due to angle of attack. F = 6; M = 0.21.

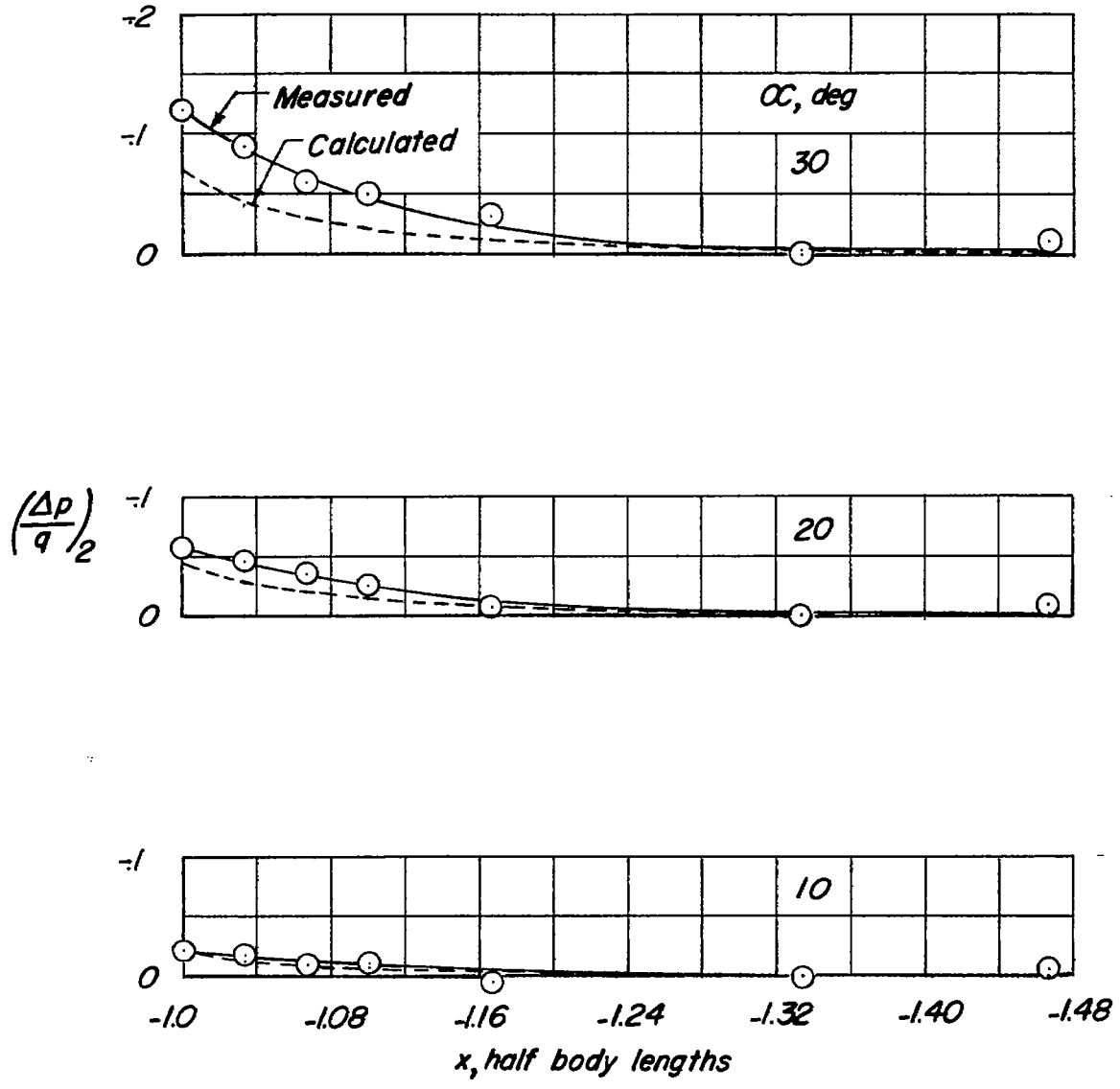

(b) Br = 0.1; θ = 180°.

Figure 18.- Continued.

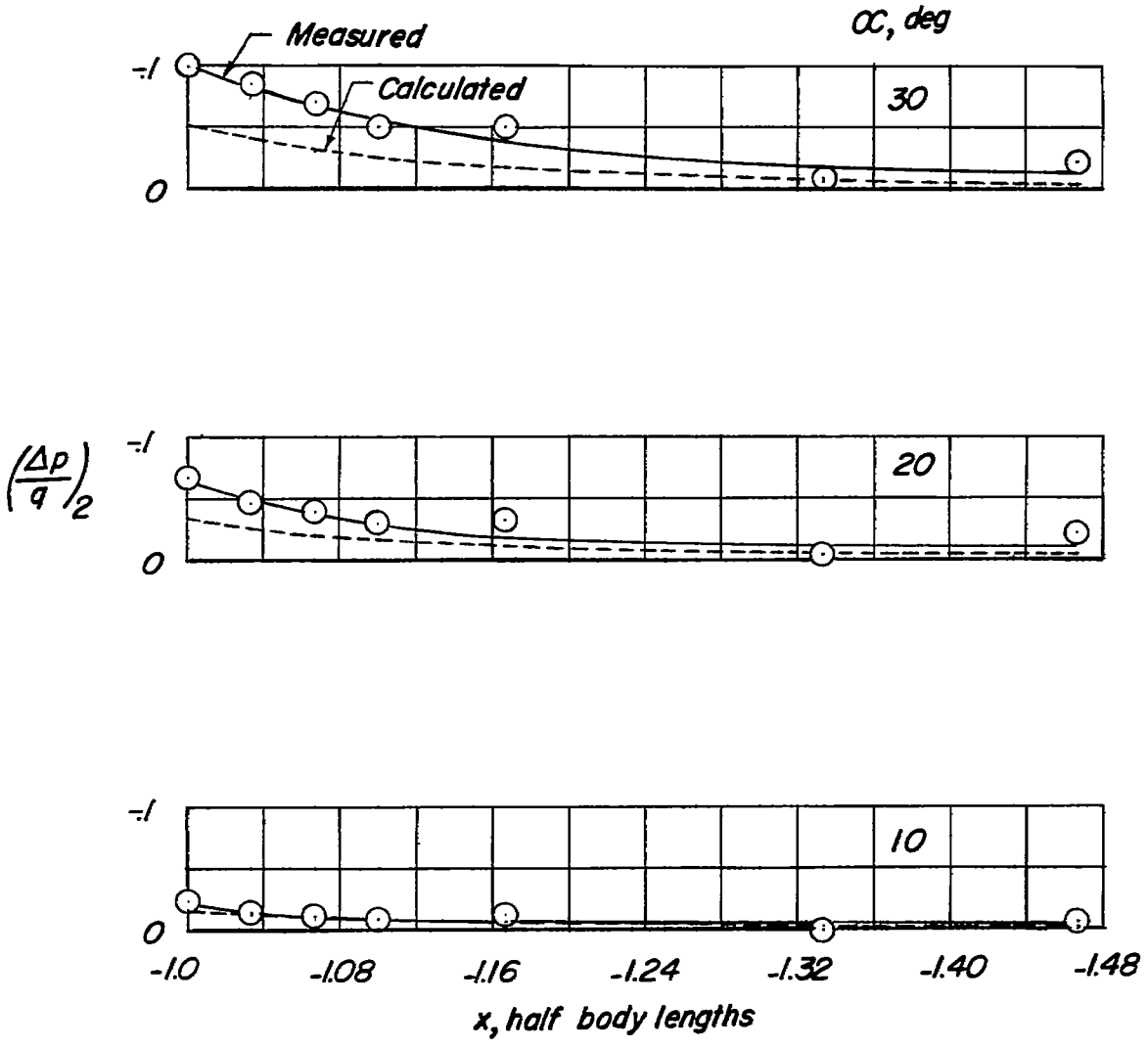

(c) Br = 0.2; $\theta = 180^{\circ}$.

Figure 18.- Continued.

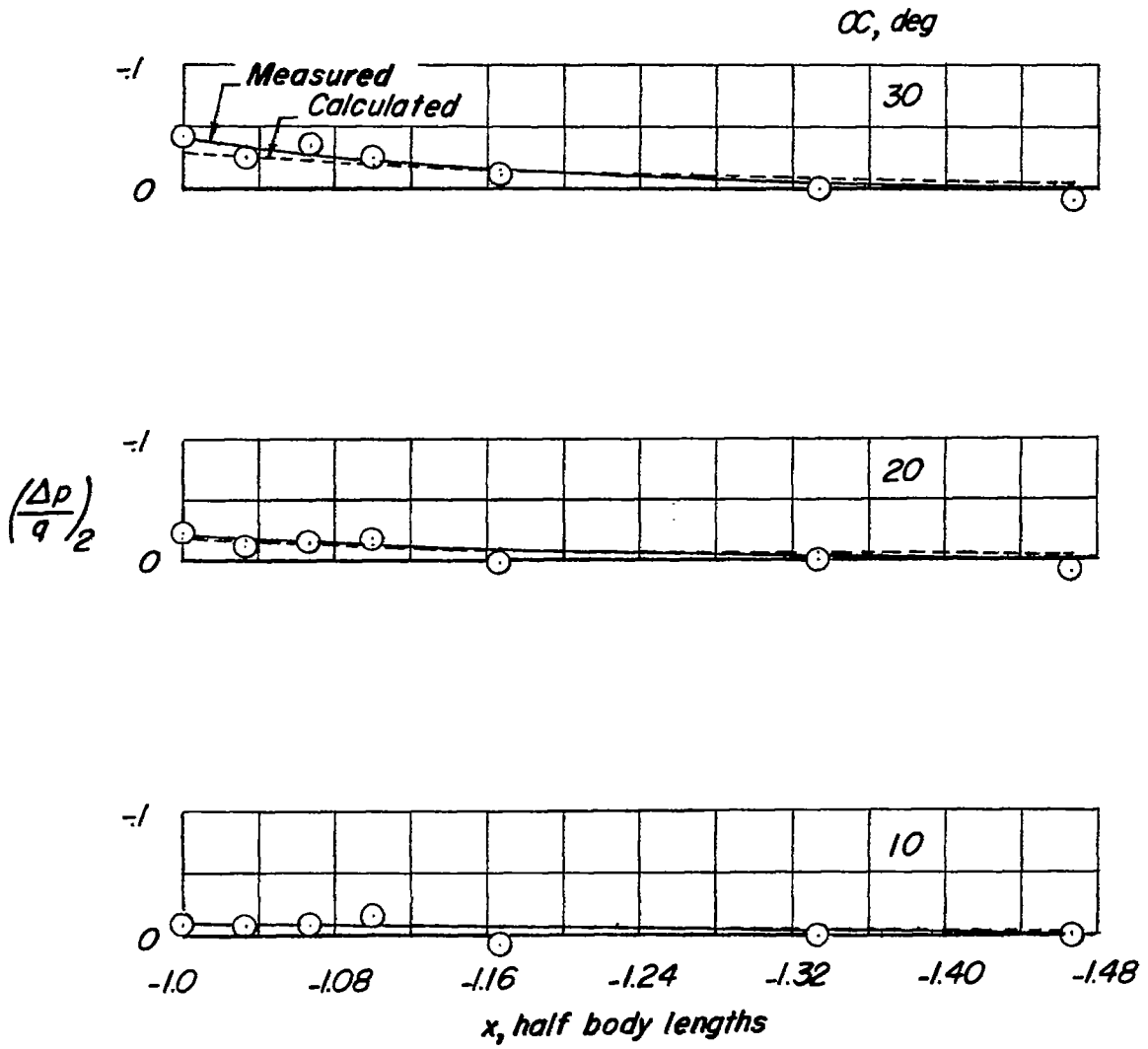

(d) Br = 0.4; θ = 180°.

Figure 18.- Concluded.

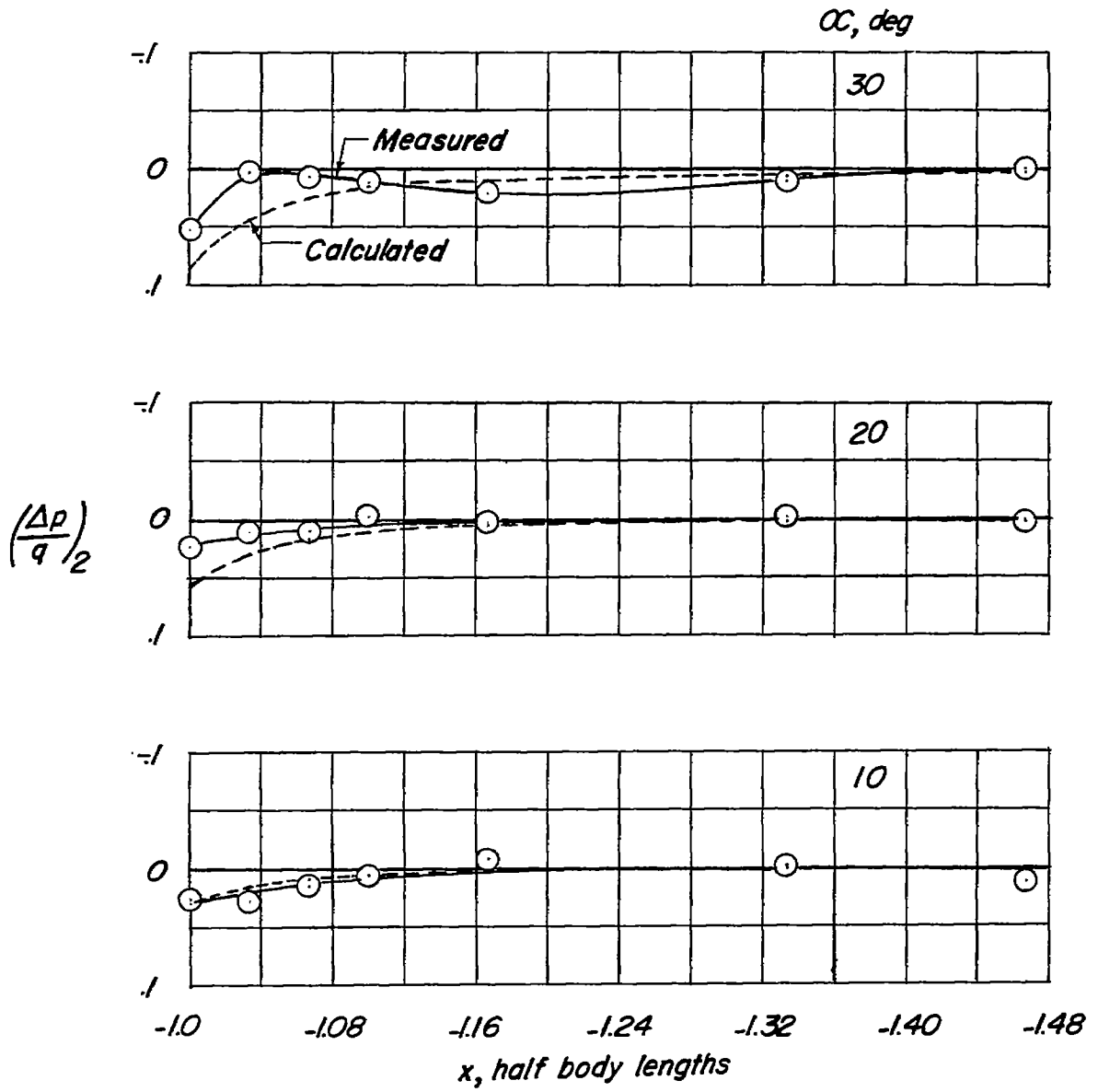

(a) Br = 0.05; $\theta = 0^{\circ}$.

Figure 19.- Comparison of the calculated and measured incremental pressure coefficient at $\theta = 0^{\circ}$ ahead of a parabolic-arc body of revolution due to angle of attack. F = 6; M = 0.21.

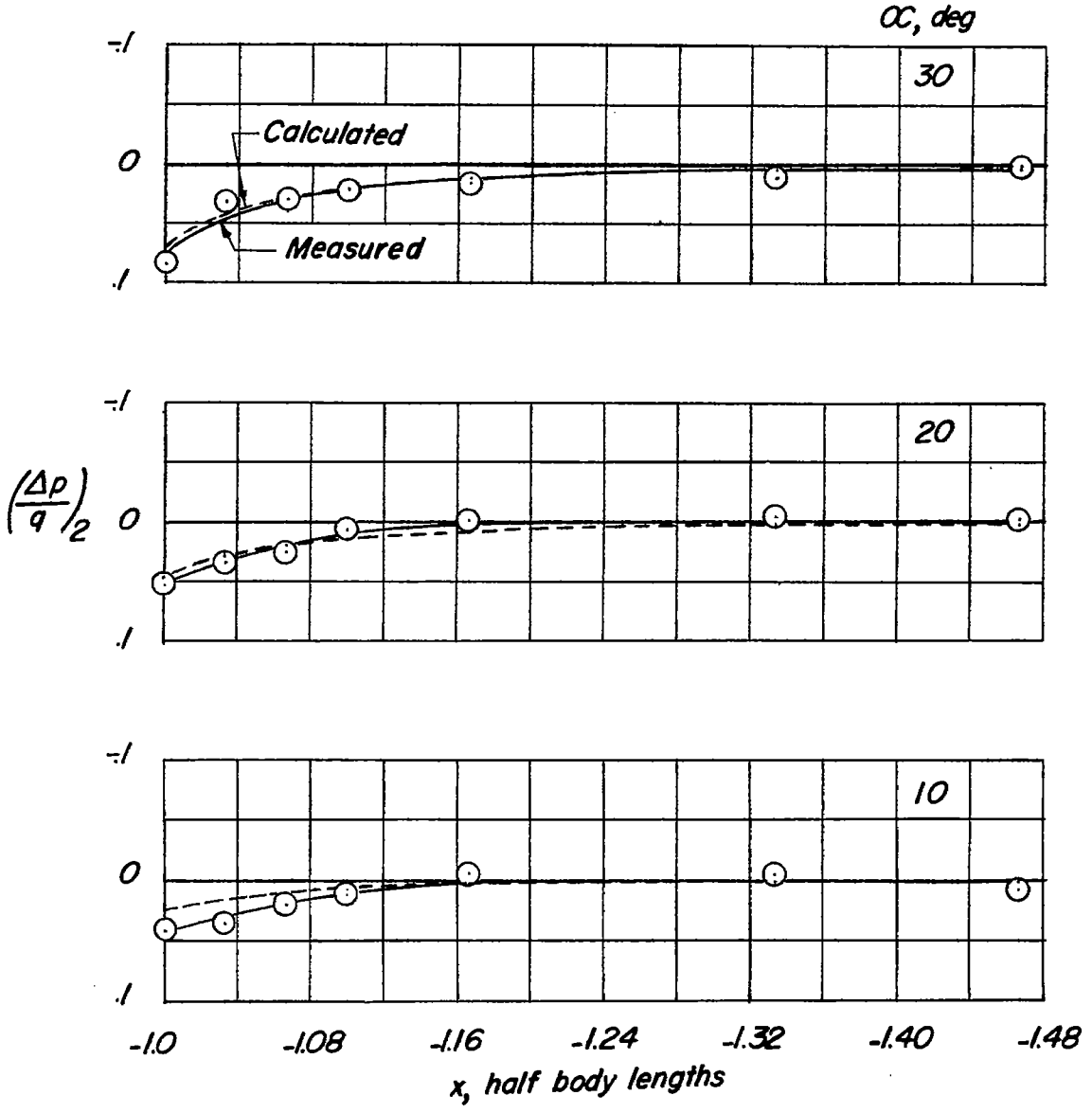

(b) Br = 0.1; $\theta = 0^{\circ}$.

Figure 19.- Continued.

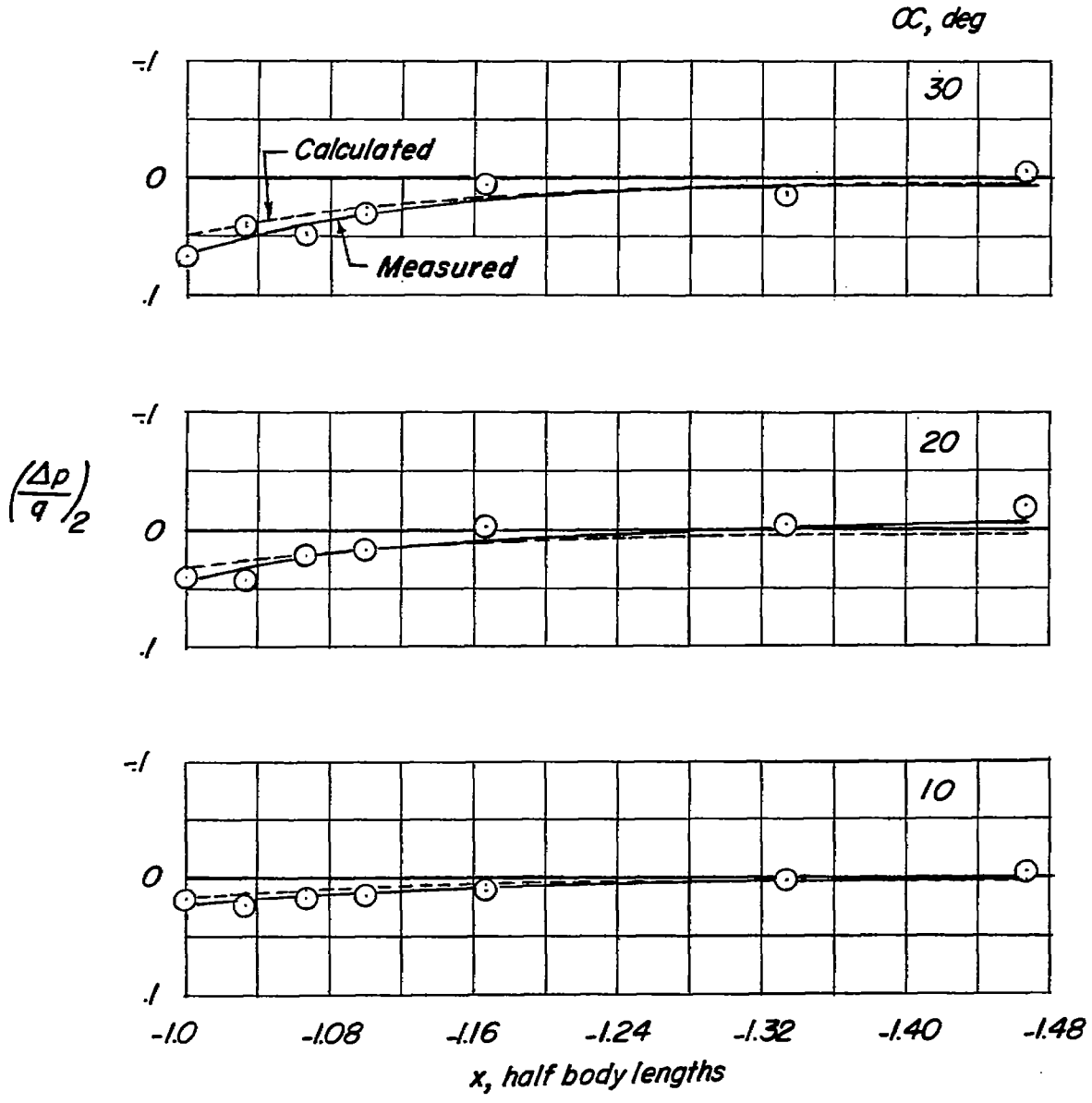

(c) Br = 0.2; θ = 0°.

Figure 19.- Continued.

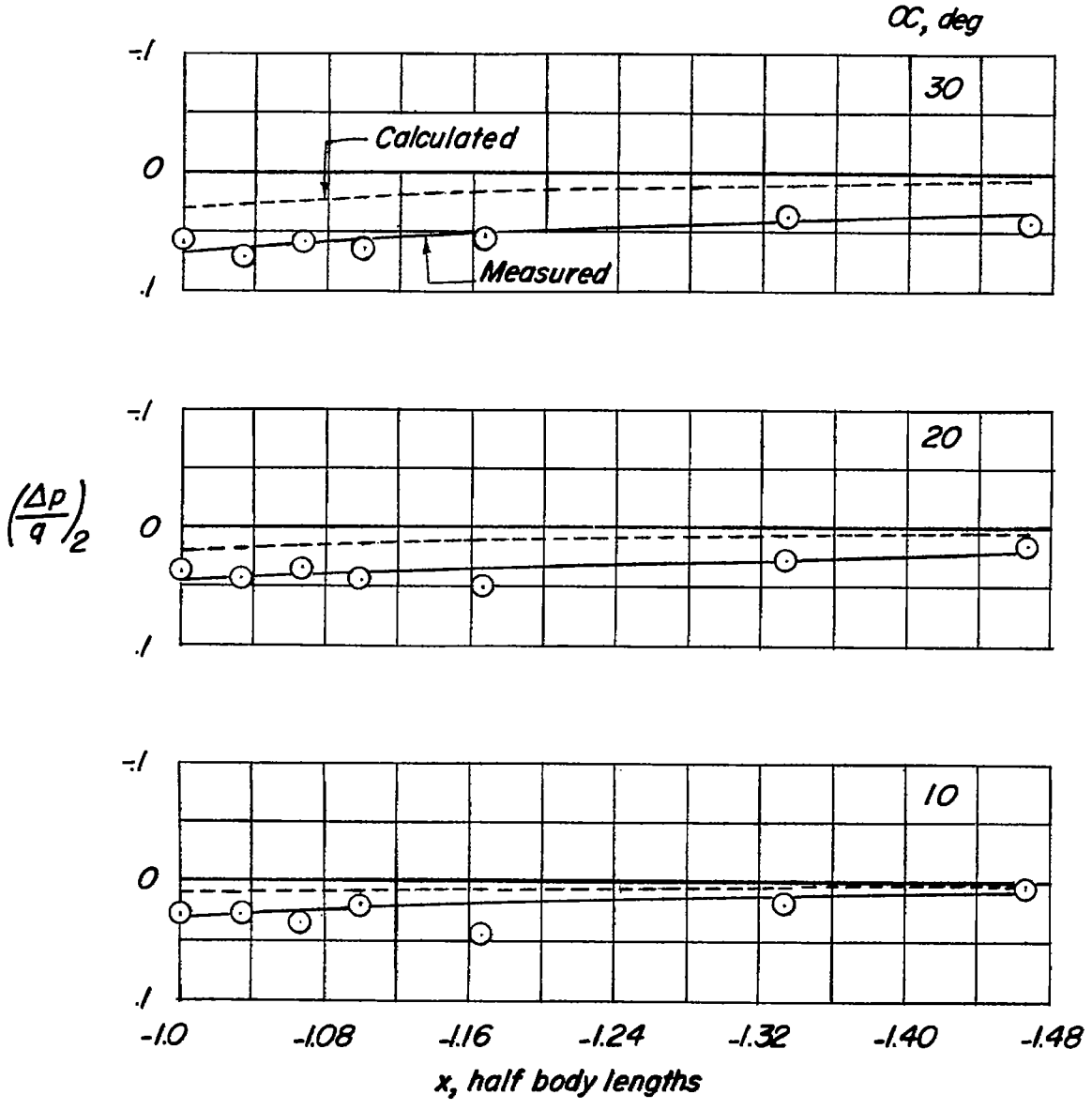

(d) Br = 0.4; $\theta = 0^{\circ}$.

Figure 19.- Concluded.

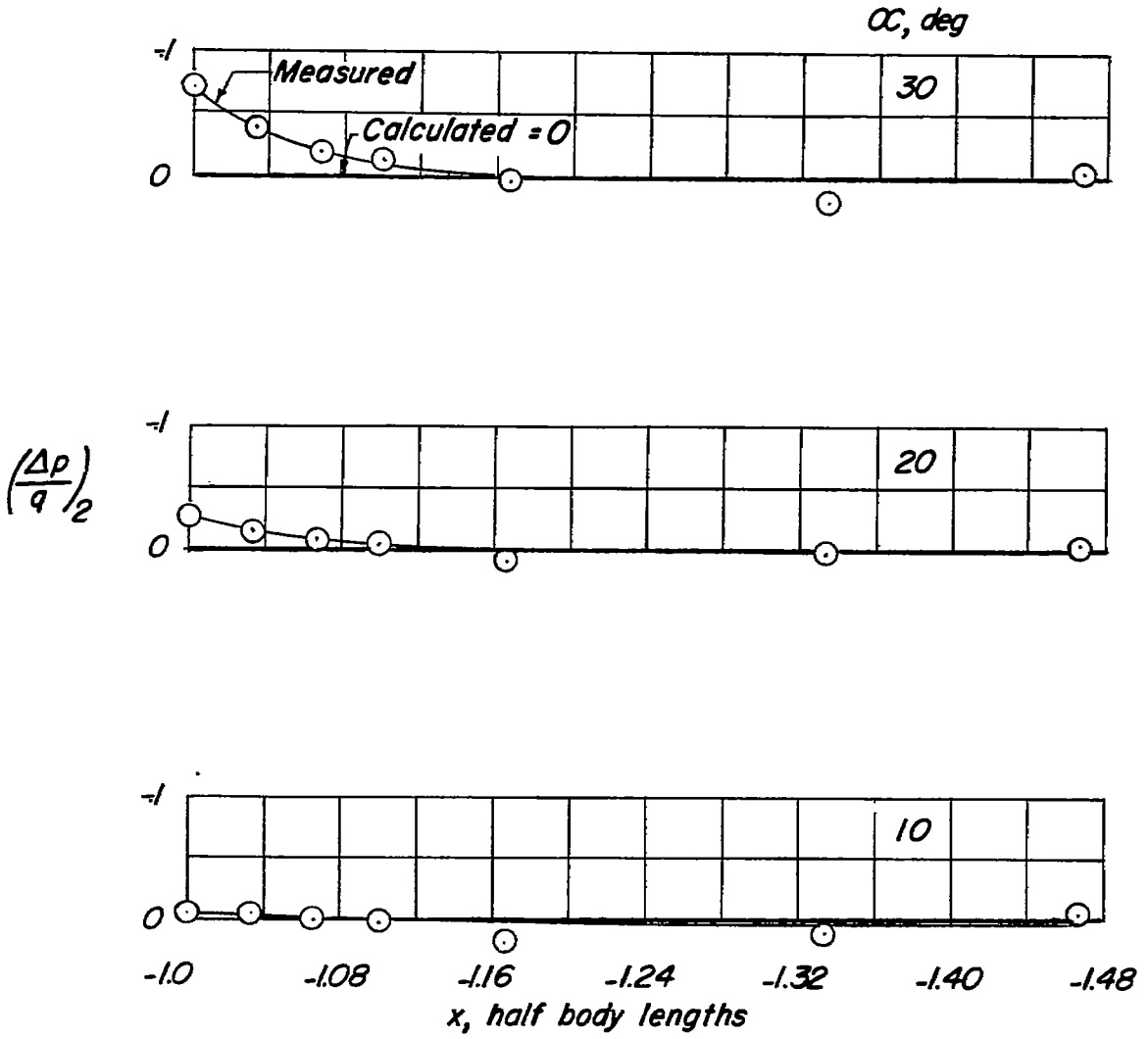

(a) Br = 0.05; $\theta = 90^\circ$.

Figure 20.- Comparison of the calculated and measured incremental pressure coefficient at $\theta = 90^\circ$ ahead of a parabolic-arc body of revolution due to angle of attack. F = 6; M = 0.21.

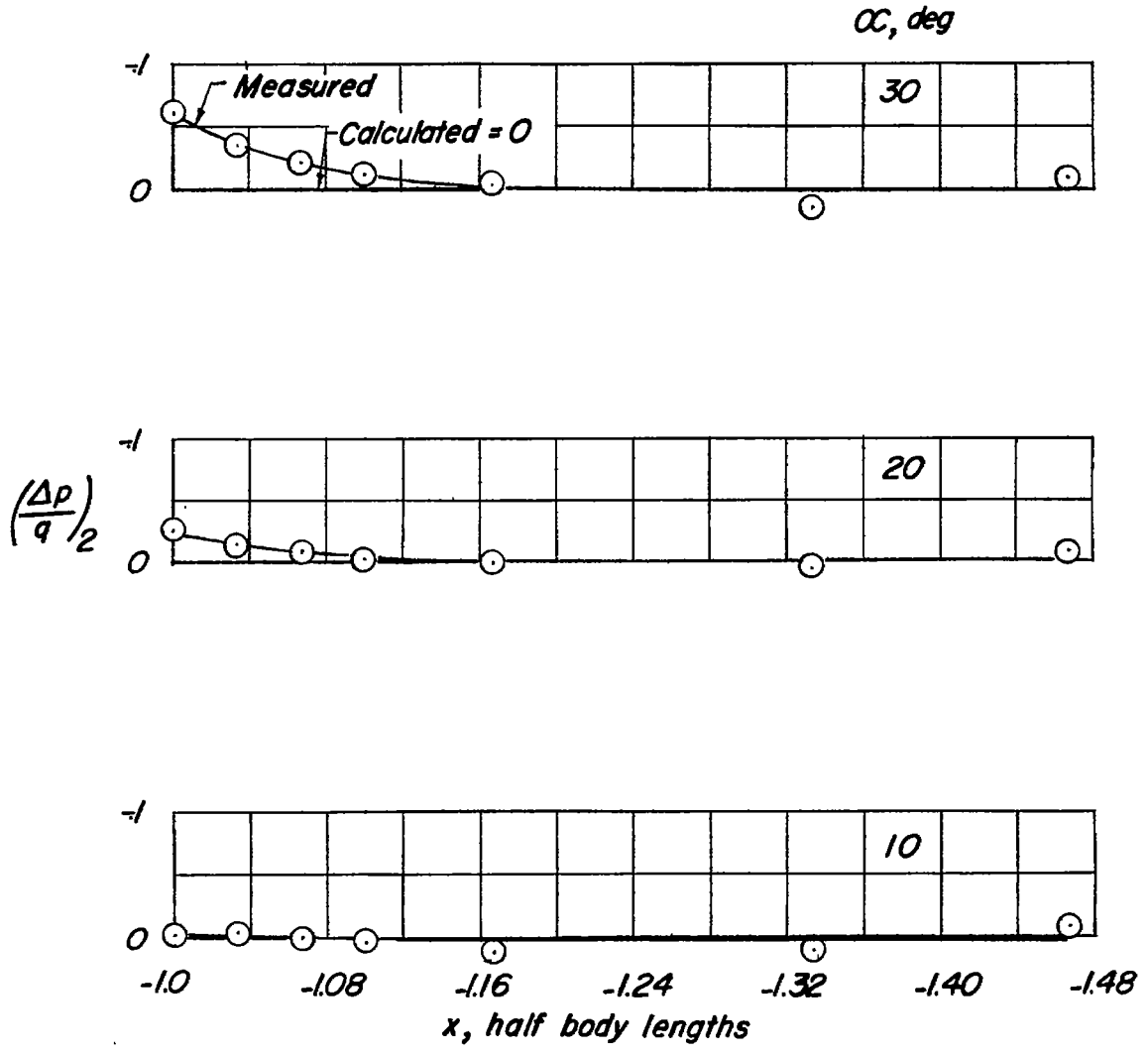

(b) Br = 0.1; $\theta = 90^\circ$.

Figure 20.- Continued.

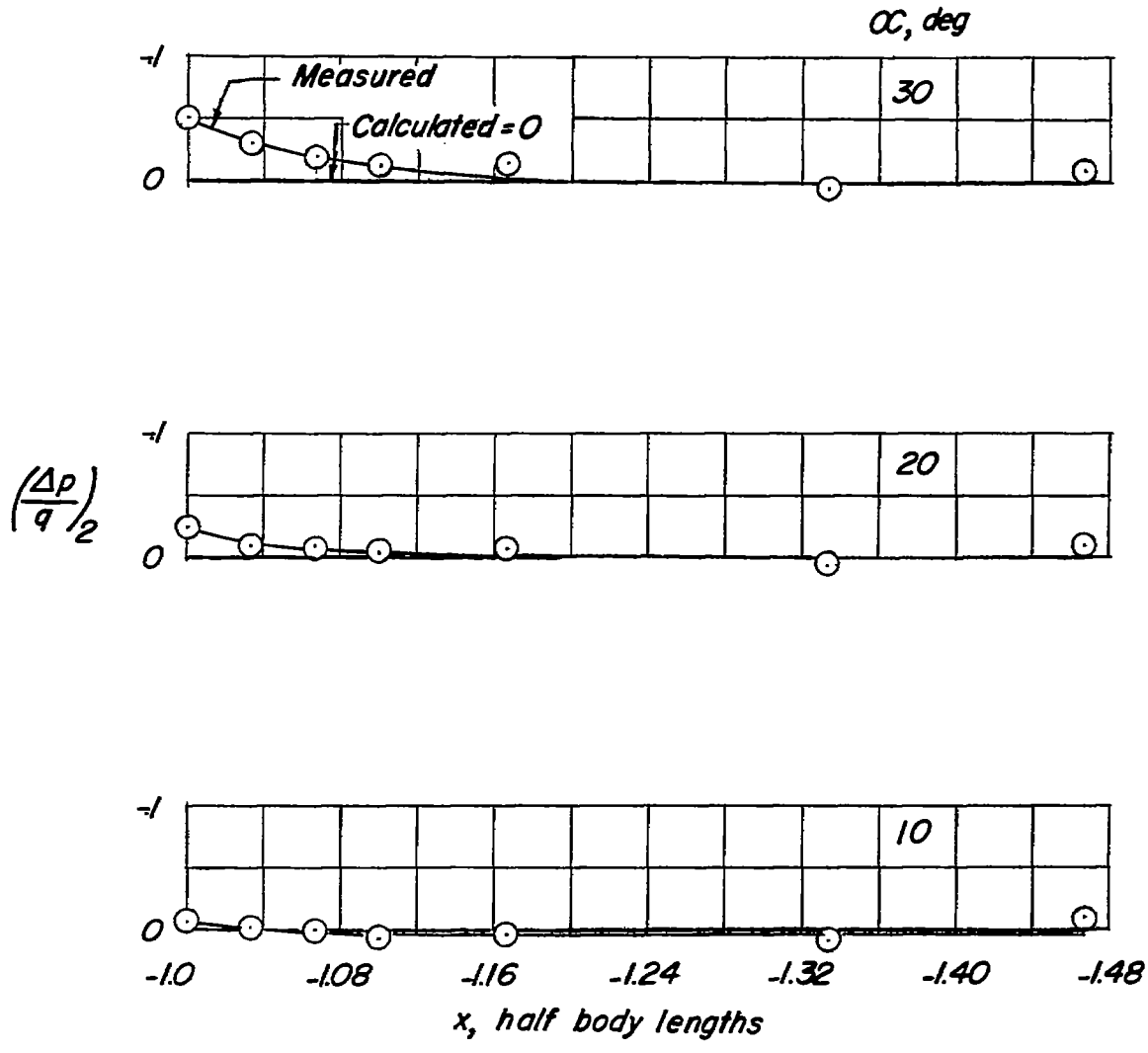

(c) Br = 0.2; $\theta = 90^\circ$.

Figure 20.- Continued.

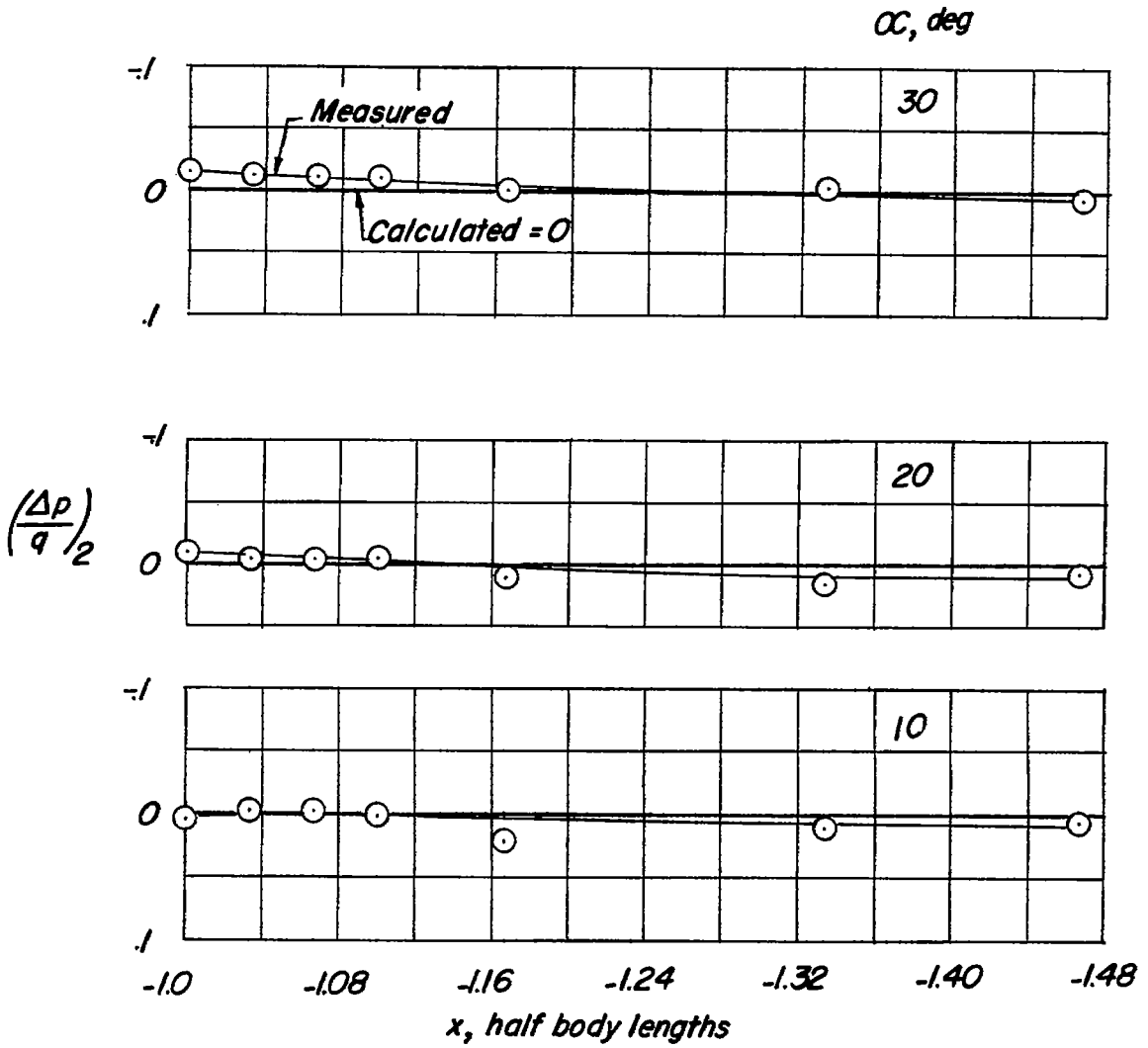

(d) Br = 0.4; $\theta = 90^{\circ}$.

Figure 20.- Concluded.

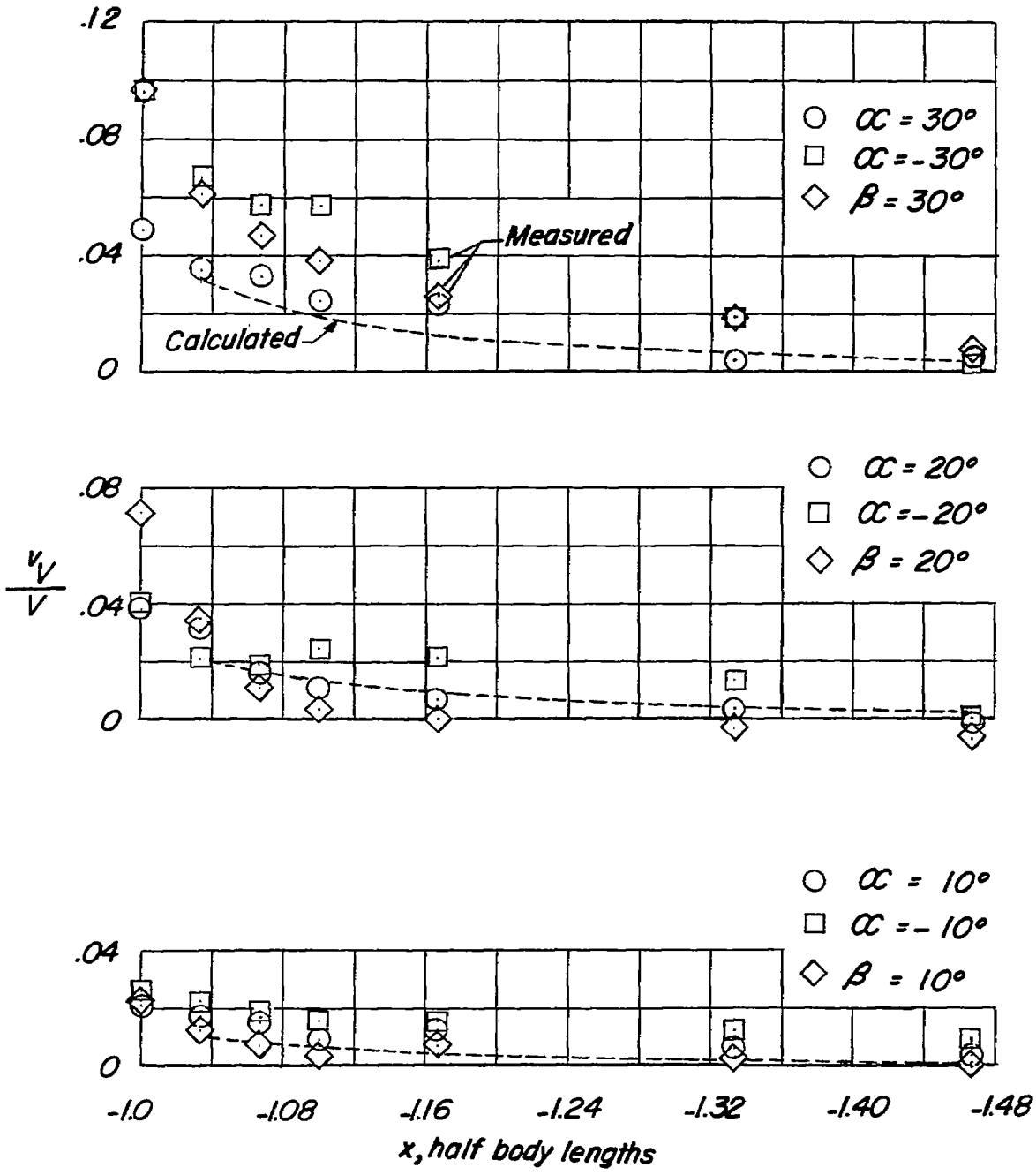

Figure 21.- Comparison of the calculated and measured change in flow inclination on the body axis ahead of a parabolic-arc body of revolution due to inclination of body. F = 6; M = 0.21.

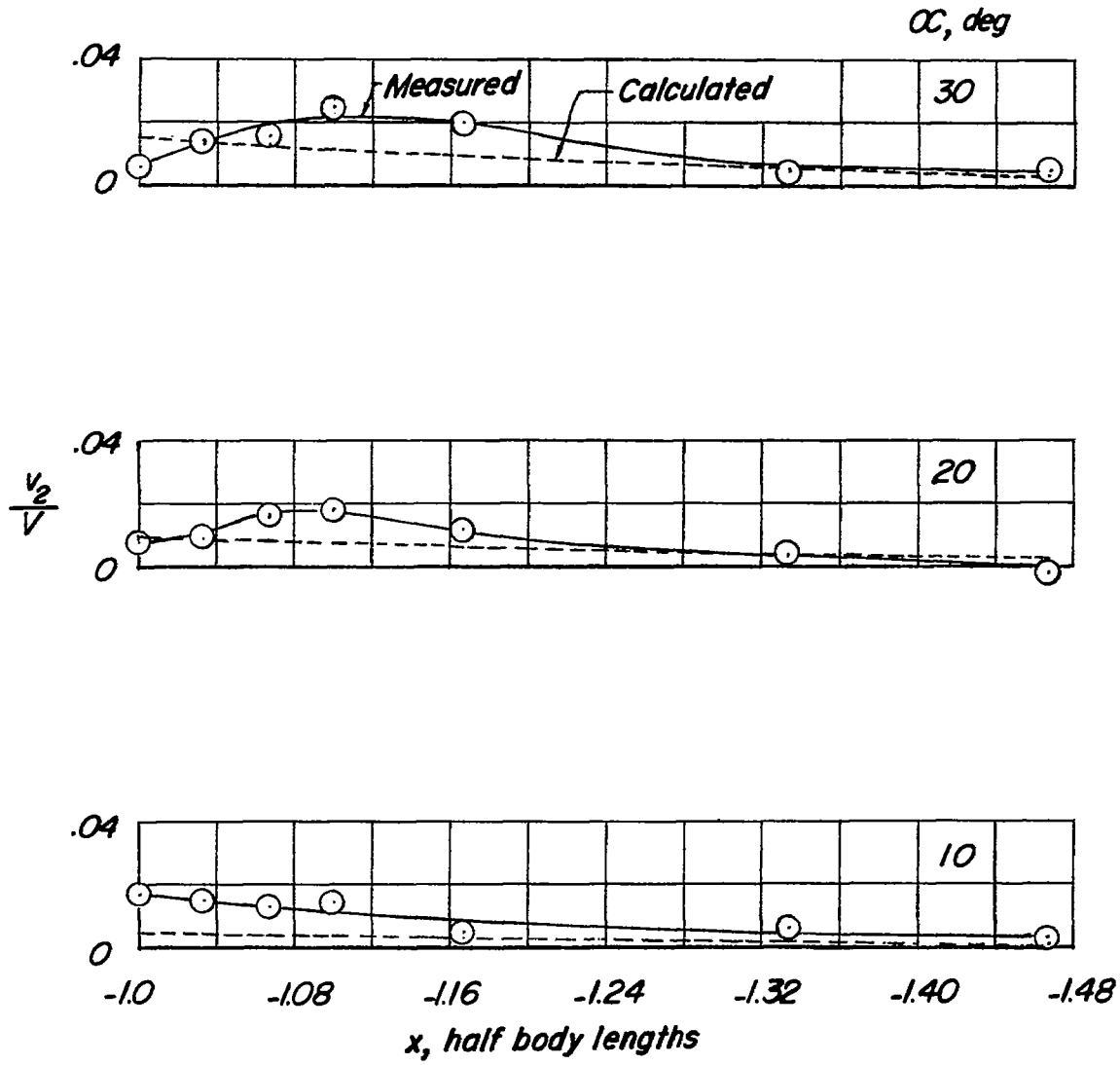

(a) Br = 0.1; $\theta = 180^{\circ}$.

Figure 22.- Comparison of the calculated and measured change in flow inclination at $\theta = 180^{\circ}$ ahead of a parabolic-arc body of revolution due to angle of attack. F = 6; M = 0.21.

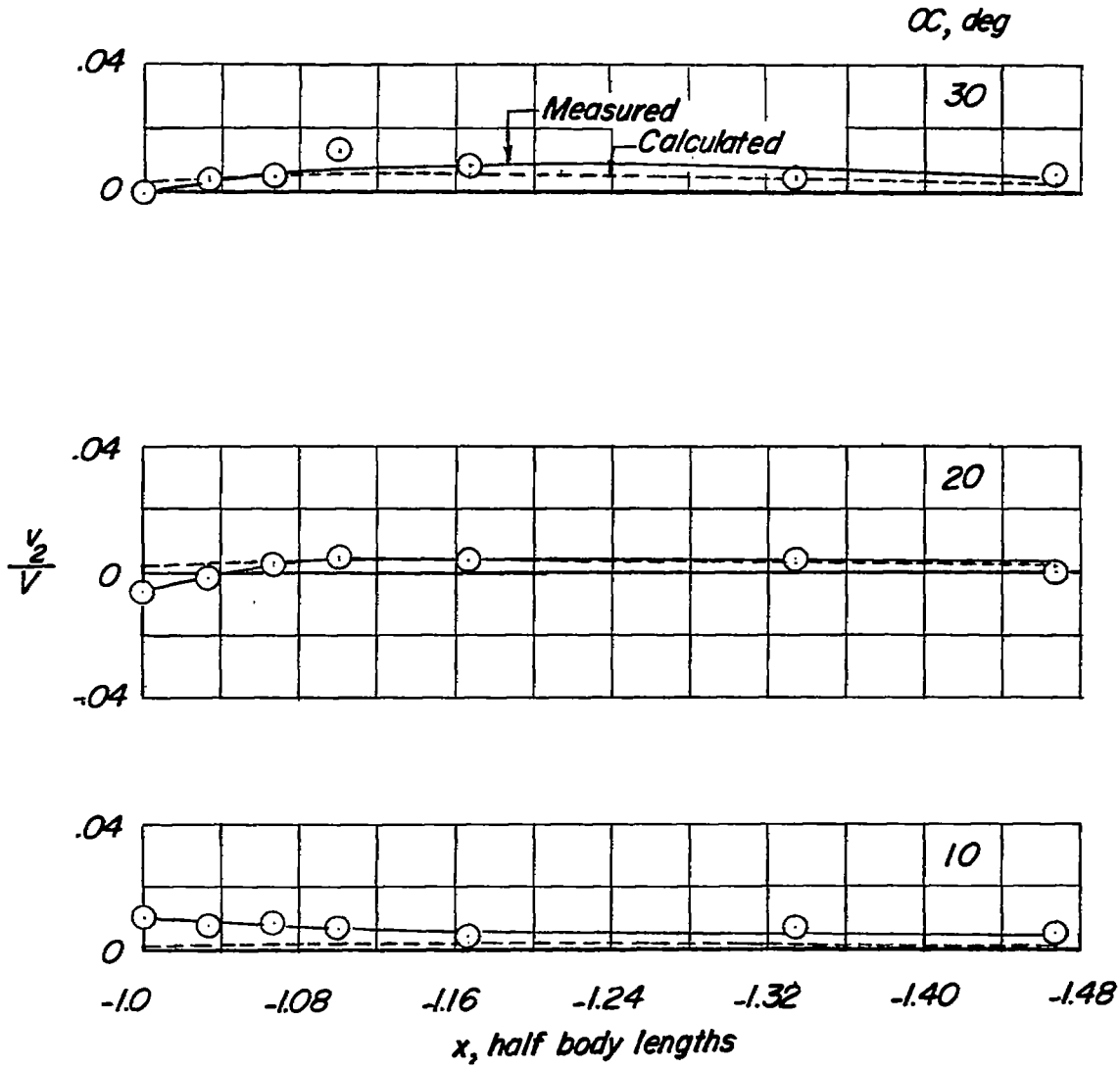

(b) Br = 0.2; θ = 180°.

Figure 22.- Continued.

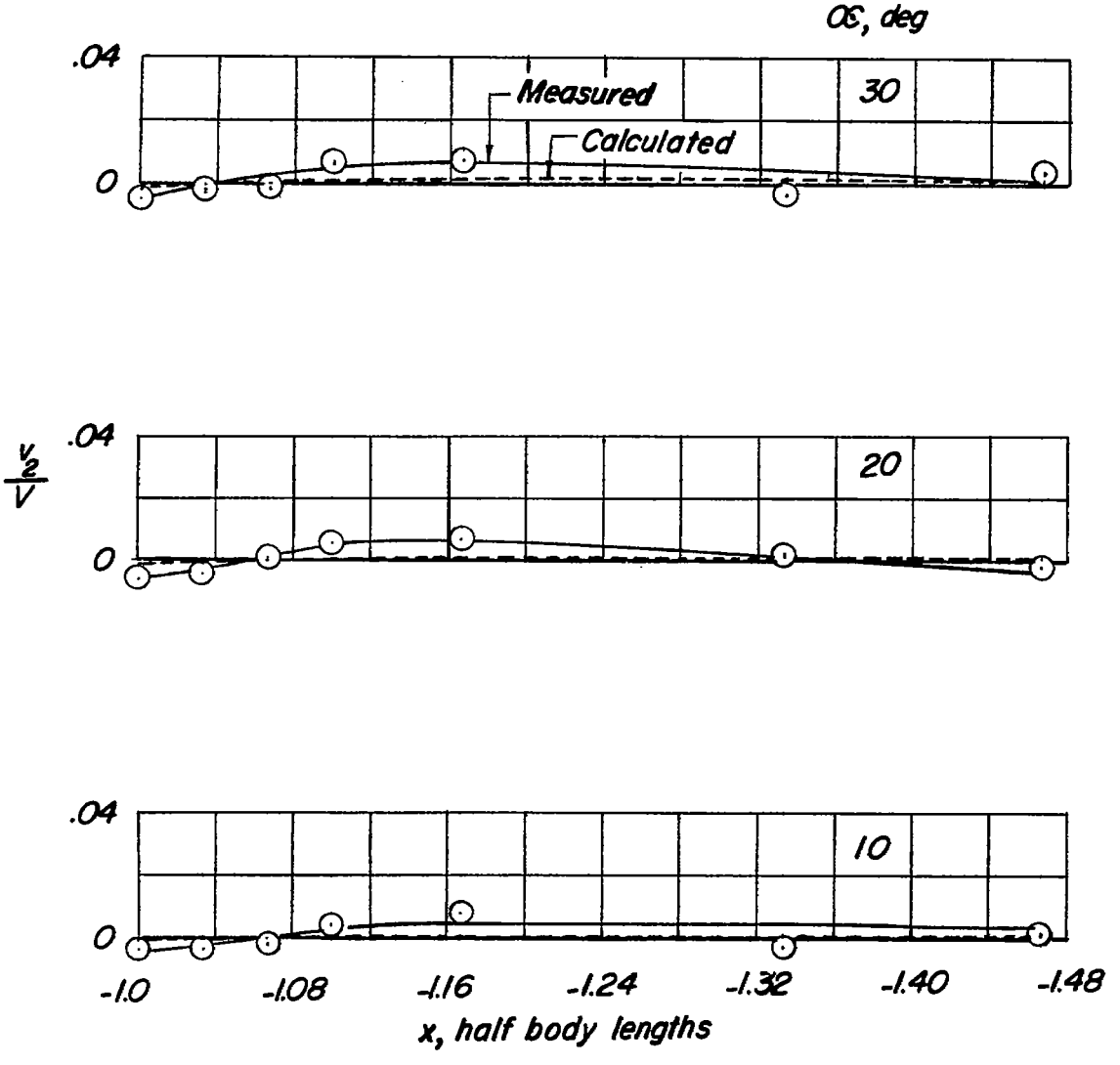

(c) Br = 0.4; θ = 180°.

Figure 22.- Concluded.

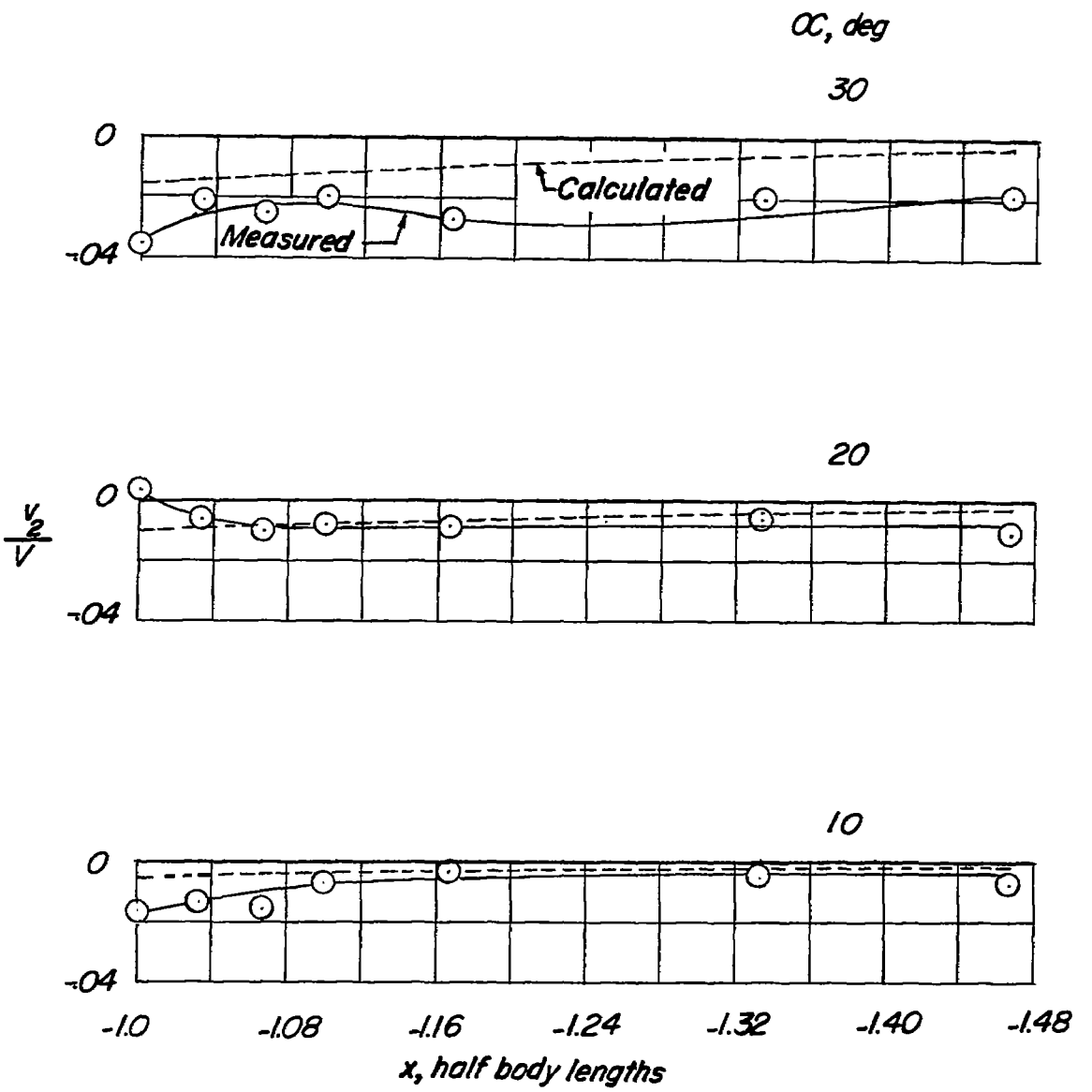

(a) Br = 0.1; θ = 0°.

Figure 23.- Comparison of the calculated and measured change in flow inclination at θ = 0° ahead of a parabolic-arc body of revolution due to angle of attack. F = 6; M = 0.21.

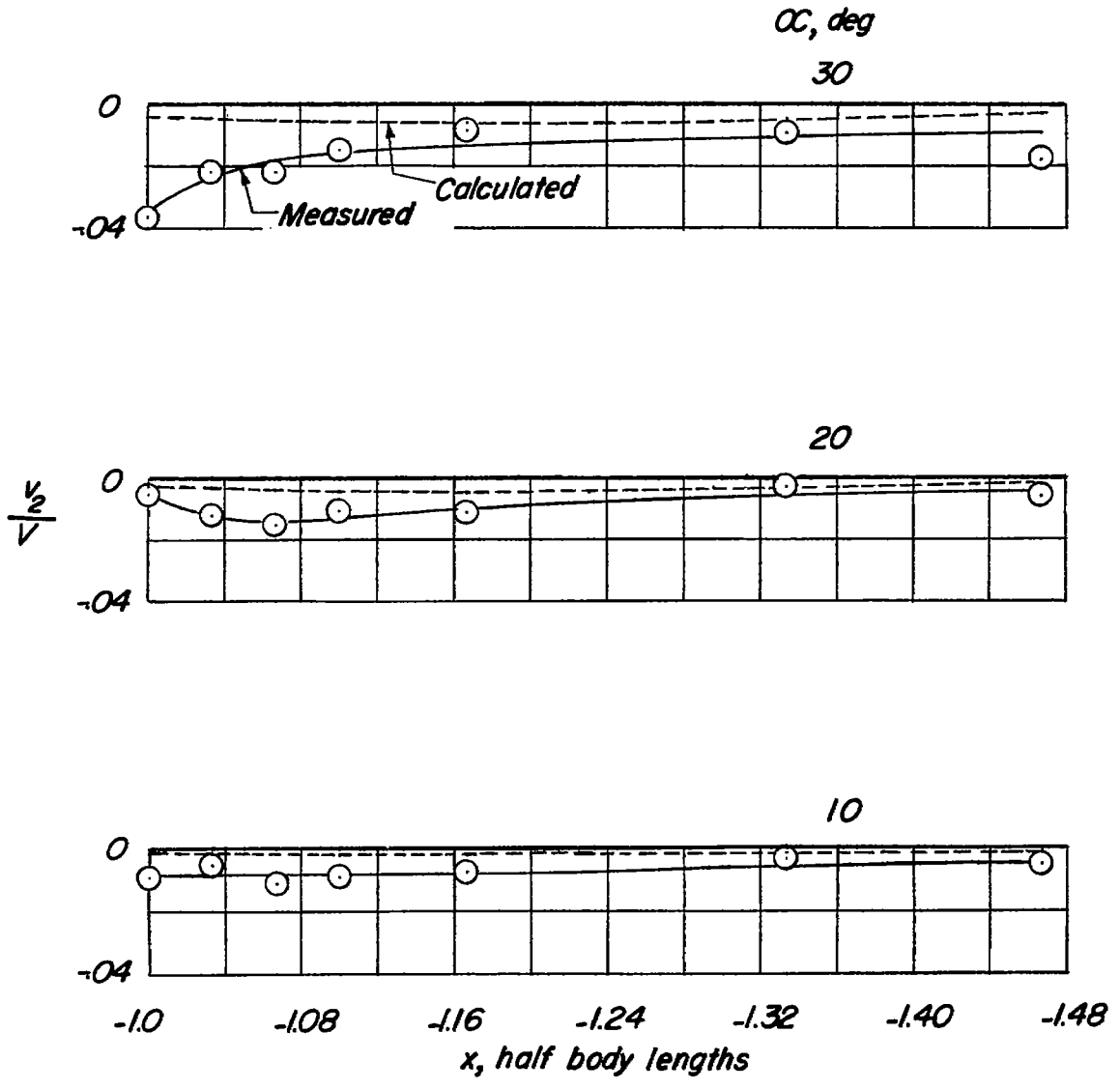

(b) Br = 0.2; $\theta = 0^{\circ}$.

Figure 23.- Continued.

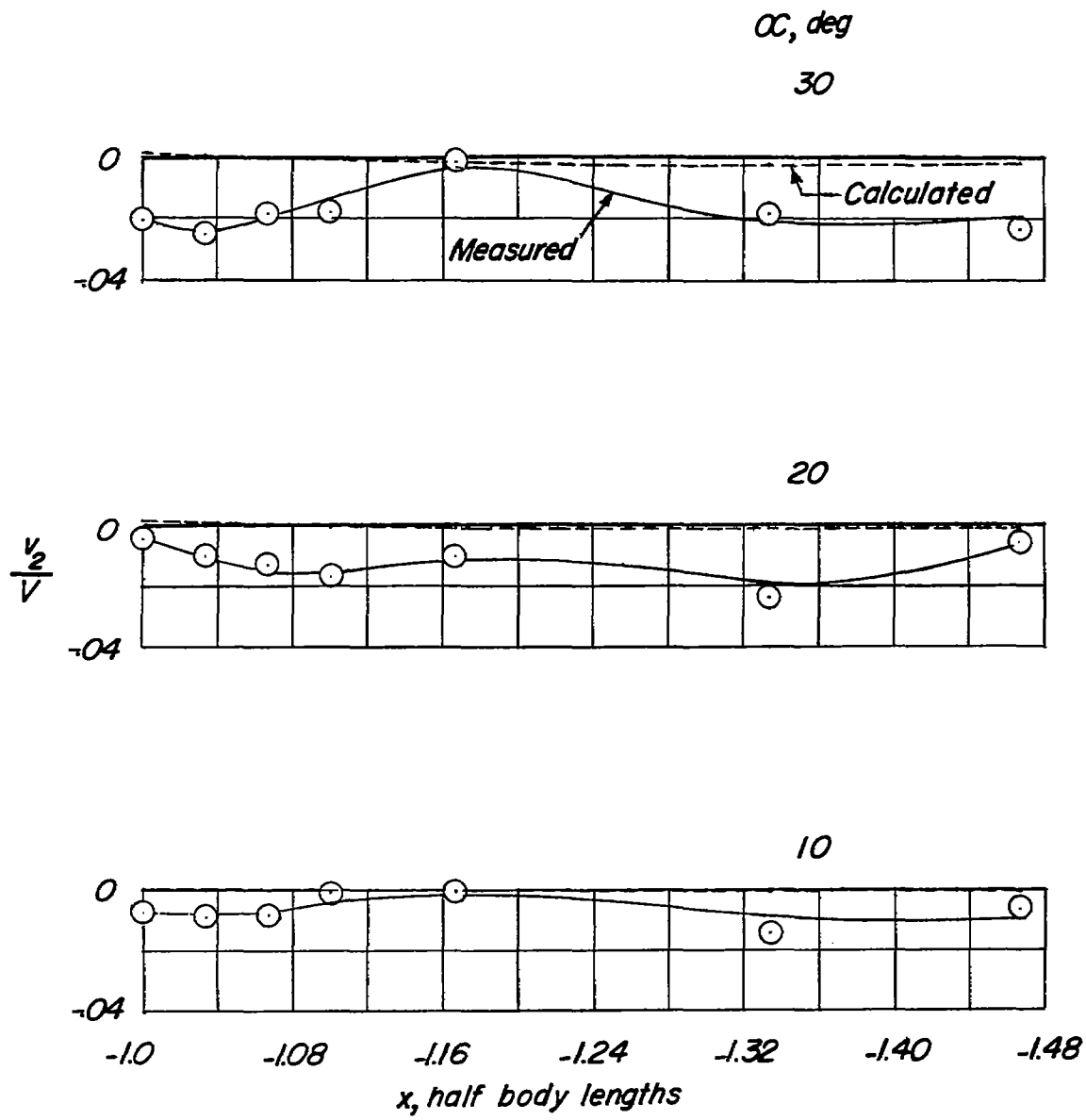

(c) Br = 0.4; $\theta = 0^{\circ}$.

Figure 23.- Concluded.

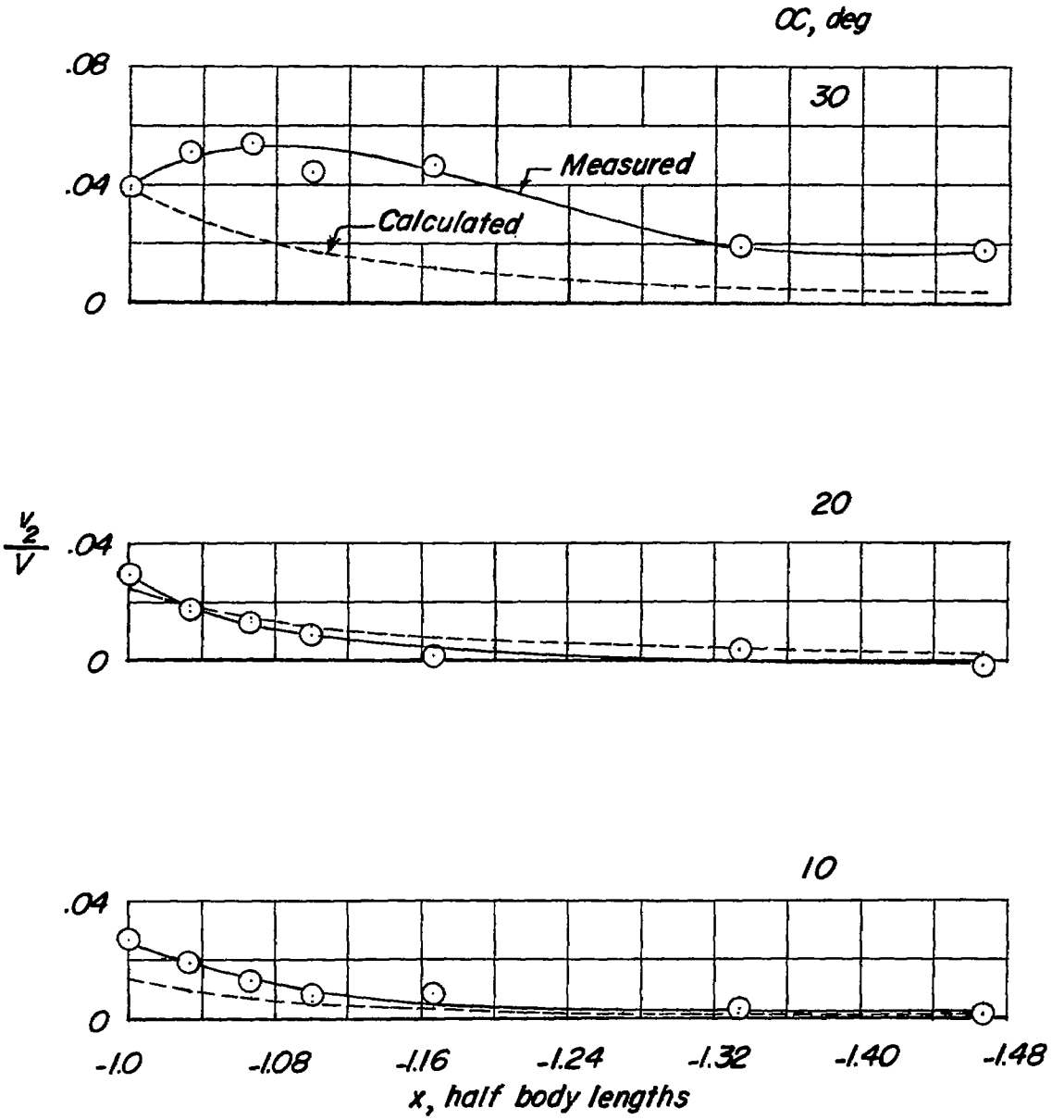

(a) Br = 0.1; $\theta = 90^{\circ}$.

Figure 24.- Comparison of the calculated and measured change in flow inclination at $\theta = 90^{\circ}$ ahead of a parabolic-arc body of revolution due to angle of attack. F = 6; M = 0.21.

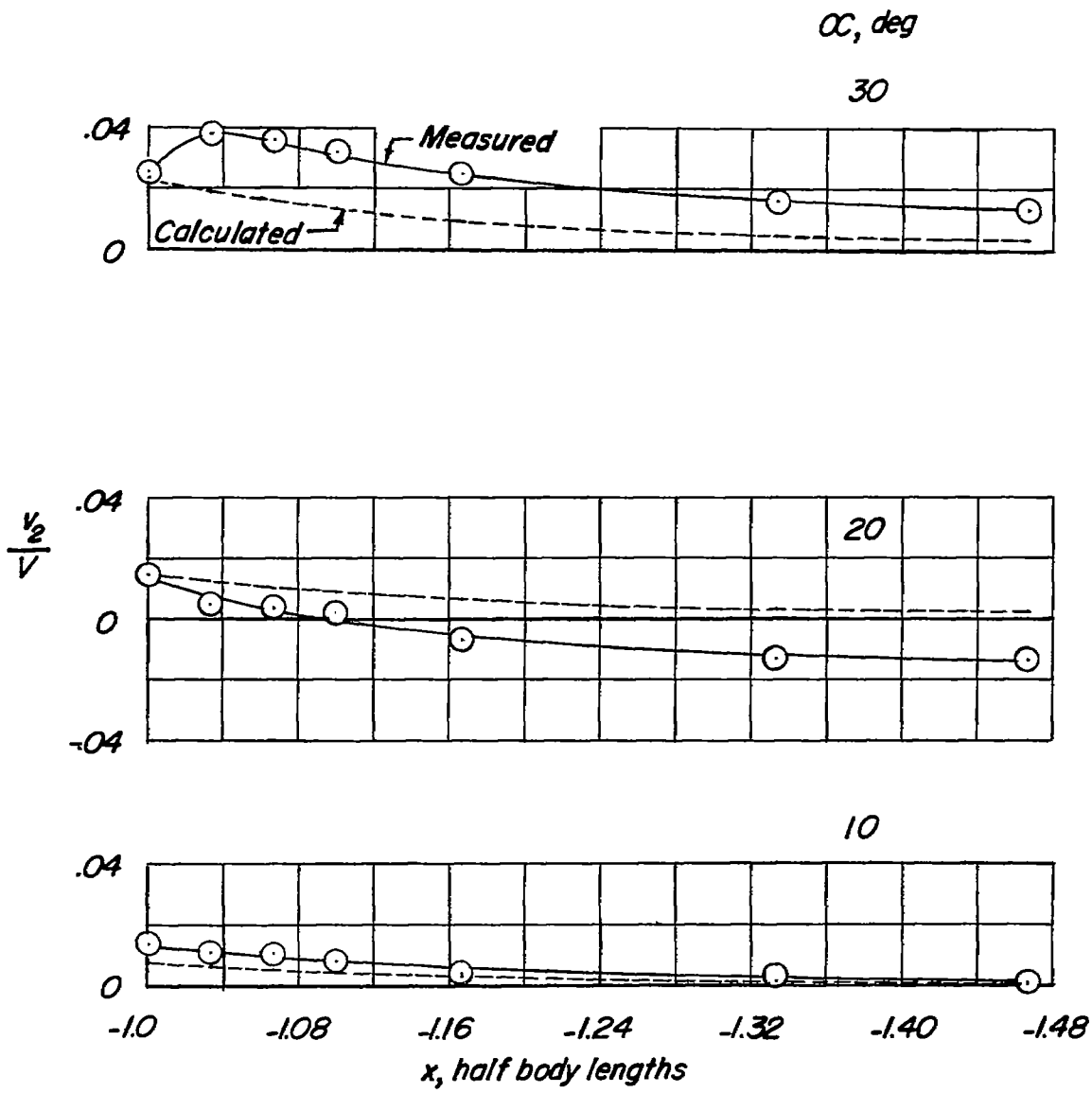

(b) Br = 0.2; θ = 90°.

Figure 24.- Continued.

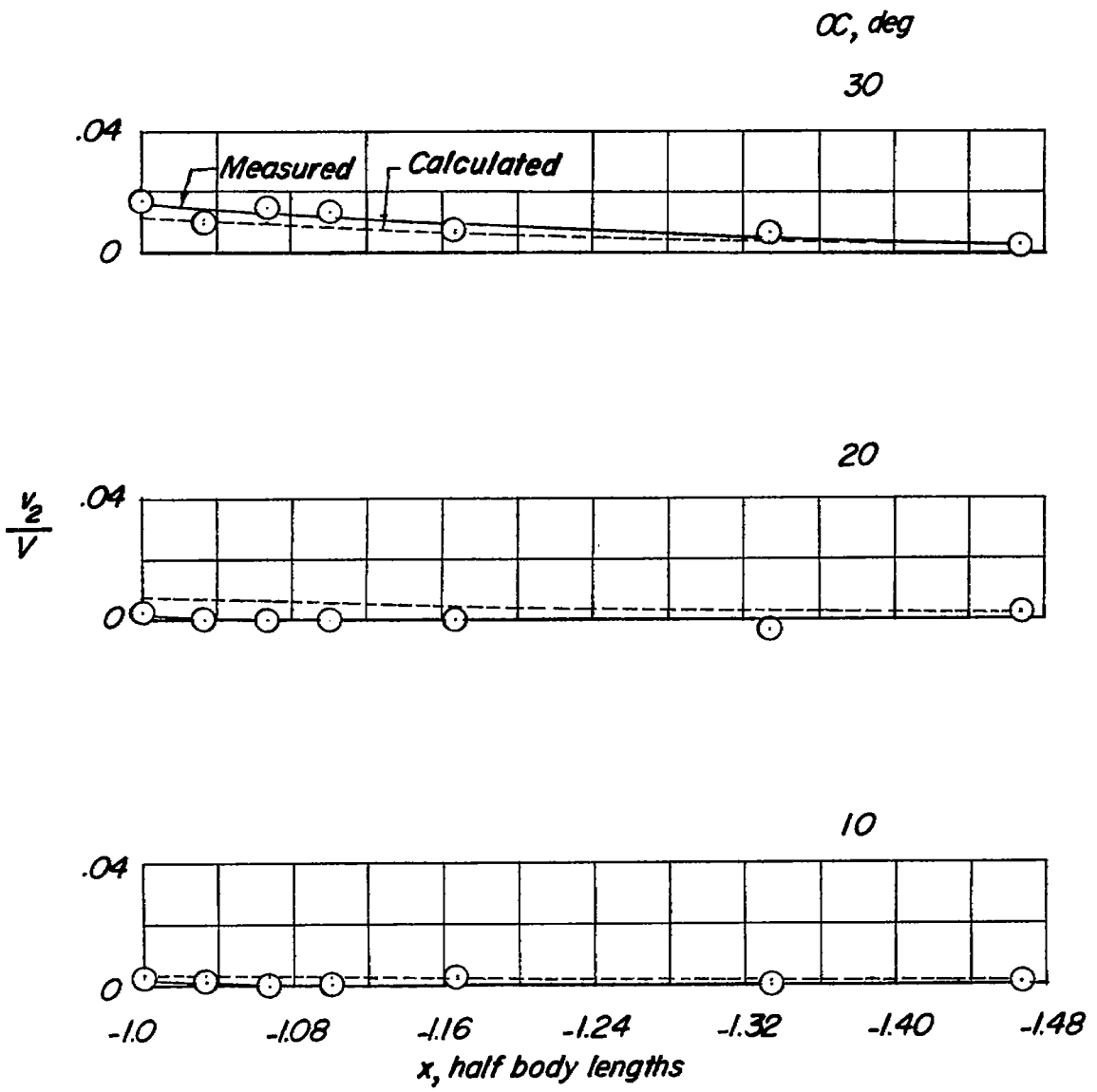

(c) Br = 0.4; θ = 90°.

Figure 24.- Concluded.